Biol Cybern (2011) 104:95–119
DOI 10.1007/s00422-011-0422-1

ORIGINAL PAPER

Biological Cybernetics

Deriving neural network controllers from neuro-biological data: implementation of a single-leg stick insect controller

Arndt von Twickel · Ansgar Büschges · Frank Pasemann

Received: 8 March 2010 / Accepted: 27 January 2011 / Published online: 15 February 2011

Abstract This article presents modular recurrent neural network controllers for single legs of a biomimetic six-legged robot equipped with standard DC motors. Following arguments of Ekeberg et al. (Arthropod Struct Dev 33:287–300, 2004), completely decentralized and sensori-driven neuro-controllers were derived from neuro-biological data of stick-insects. Parameters of the controllers were either hand-tuned or optimized by an evolutionary algorithm. Employing identical controller structures, qualitatively similar behaviors were achieved for robot and for stick insect simulations. For a wide range of perturbing conditions, as for instance changing ground height or up- and downhill walking, swing as well as stance control were shown to be robust. Behavioral adaptations, like varying locomotion speeds, could be achieved by changes in neural parameters as well as by a mechanical coupling to the environment. To a large extent the simulated walking behavior matched biological data. For example, this was the case for body support force profiles and swing trajectories under varying ground heights. The results suggest that the single-leg controllers are suitable as modules for hexapod controllers, and they might therefore bridge morphological- and behavioral-based approaches to stick insect locomotion control.

Keywords Walking control · Robotics · Neural network · Sensori-motor loops

1 Introduction

Over the last decades substantial progress has been made in research on walking machine control (Bekey 2005) and neuro-biological control mechanisms of walking in animals (Orlovsky et al. 1999; Büschges et al. 2008). Despite this progress, knowledge about the interaction of sensori-motor loops in walking control (on the neural level) remains limited. This becomes increasingly obvious when going from intra-joint to intra-leg to inter-leg coordination of movement. This is, among others, due to: (1) The complexity of walking systems, consisting not only of distributed (neural) control systems but also of biomechanics, sensor- and motor-systems, and diverse environmental conditions (embodiment and situatedness, see e.g., Hatsopoulos 1996; Chiel et al. 2009; Pfeifer and Bongard 2006). (2) The difficulty of recording multiple neuronal activations under artificial and "reduced" walking conditions, not to speak of diverse "natural" conditions (Ritzmann and Büschges 2007). (3) The lack of formal tools to describe the functionality of sensori-motor control in non-linear closed feedback loops and to determine a behavior relevant coupling of these feedback loops. This is in contrast to standard control techniques, using, e.g., coupled Central Pattern Generators (CPGs) or trajectory control (Ijspeert 2008; Azevedo et al. 2007).

In addition to detailed biological experiments, whole system approaches (Webb 2009, cp. and comments in same issue) integrating the detailed data in, e.g., simulation studies

Electronic supplementary material The online version of this article (doi:10.1007/s00422-011-0422-1) contains supplementary material, which is available to authorized users.

A. von Twickel (✉) · F. Pasemann
Department of Neurocybernetics, Institute of Cognitive Science, University of Osnabrück, 49069 Osnabrück, Germany
e-mail: avontwic@uos.de

A. von Twickel · F. Pasemann
Institute for Advanced Study, Wallotstraße 19, 14193 Berlin, Germany

A. Büschges
Department of Animal Physiology, Zoological Institute, University of Cologne, 50674 Cologne, Germany

(Pearson et al. 2006) are needed to: (1) Test if the collected data is sufficient to generate the behavior under study. (2) Systematically "play" with parameters and alternative control mechanisms to generate new hypotheses about mechanisms of sensori-motor couplings. This will guide subsequent experimental research. (3) Derive new control techniques for walking machines. A promising tool to explore parameter space in this context is, e.g., evolutionary robotics (Nolfi and Floreano 2000; Beer 2006; von Twickel and Pasemann 2007).

One of the best studied organisms regarding walking control, especially on the neural level, is the stick insect: on the one hand, sufficient knowledge about the neural mechanisms underlying single-leg stepping control has been gathered (Büschges 2005; Bässler and Büschges 1998) to reproduce stepping behavior in simulation (Ekeberg et al. 2004) and on robotic models (Lewinger et al. 2006). On the other hand, inter-leg coordination rules based on behavioral data have been proposed ("Cruse rules," see Cruse 1990), quantified in different behavioral contexts (Dürr 2005) and intensively tested in simulations and on robots (e.g., Dürr et al. 2004; Calvitti and Beer 2000). First neurobiological data related to inter-leg coordination were published by Brunn and Dean (1994) from standing stick insects. The interpretation of these results was in particular useful for hypothesizing potential neural control features underlying spatial coordination in walking (for details see, Dürr et al. 2004). More recent data on neural inter-leg coordination from walking stick insects (Ludwar et al. 2005; Borgmann et al. 2009, 2007) does neither directly support nor reject the Cruse rules. Therefore, the single-leg stick insect controller model based on neural data ("Ekeberg controller", see, Ekeberg et al. 2004) is promising to serve as a link between behavioral-based hexapod controllers ("functional" approach) and neuro-biological findings of single-leg control mechanisms and inter-leg coupling influences ("morphological" approach).

Building (modular neural) models of biological locomotion control has a long standing tradition. Models exist for controllers of, e.g., stick insects (single legs: Cruse 1980; Schumm and Cruse 2006, and hexapods: Cruse et al. 2007; Beer et al. 1997), cockroaches (Pearson and Iles 1973; Beer et al. 1997), cats (Pearson et al. 2006; Yakovenko et al. 2004; Frigon and Rossignol 2006; Maufroy et al. 2008, usually restricted to two legs), lampreys (Grillner 2006), and salamanders (Ijspeert et al. 2007). The subject of this study was the Ekeberg single-leg stick insect controller. Compared to the above-mentioned controllers its uniqueness is due to the combination of two factors: first, it is almost solely based on neuro-biological data. Second, it has a modular structure whereby the modules are coupled via the sensori-motor loop, generating the basic walking pattern without ongoing activity determined by a central pattern generator. Similar to the study described here, many of the above-mentioned controllers were developed to be deployed on a physical walking machine (e.g., Beer et al. 1997; Maufroy et al. 2008; Ijspeert et al. 2007).

To discuss sensori-motor control mechanisms in a more general setting here, the Ekeberg controllers for front-, middle-, and hind-legs were implemented as modular neural networks. This simplifies their comparison with a variety of other neuro-controllers, their usage as initial modules in modular artificial evolution (see, e.g., Hülse et al. 2007; von Twickel and Pasemann 2007) and their deployment on physical robots. The translated single-leg controllers were tested on a physical simulation of the modular walking machine Octavio[1] and validated on a simulated stick insect. Tests were performed under different perturbations, especially, considering multiple environmental conditions. Some aspects of the controllers performance, like velocity control by parameter variation and swing trajectory dependence on initial swing conditions, were analyzed in detail. The results are discussed in the context of biological data of the stick insect as well as in the context of other stick-insect like controllers. Finally, an outlook on future studies is given.

2 Materials and methods

2.1 Ekeberg controller

The Ekeberg controller model (see Fig. 1) is based on the following hypotheses: (1) each of the three main leg joints Thorax-Coxa (ThC), Coxa-Trochanter (CTr), and Femur-Tibia (FTi) possesses its own autonomous control module, generating alternating activity in the antagonistic motor neuron pools via a bistable element (Bässler and Büschges 1998). (2) Central connections are not sufficient to generate stable phase to phase inter-joint coupling, rather sensory signals can influence the generation of motor activity in two ways: (a) by directly inducing transitions in the bistable elements ("timing influence") and (b) by modifying the magnitude of the motor outputs ("magnitude influence") (Bässler and Büschges 1998).

As an example the CTr joint controller will be explained, hereafter, for the remaining two joints ThC and FTi please, see Fig. 1. An in-depth explanation, including event sequence diagrams not shown here, and detailed references are given in Ekeberg et al. (2004). The CTr joint controller may be in either of two states (levation or depression) and sensory signals determine which of the states is active ("timing influence"). If, on the one hand, the femoral chordotonal organs (fCO) signal FTi-joint (γ) extension below 70°, depressor state is activated. If, on the other hand, fCOs signal γ flexion above 120° or if TC-joint position (α) sensors signal advanced retraction below −25° or leg load sensors signal

[1] see also http://www.ikw.uos.de/~neurokybernetik.

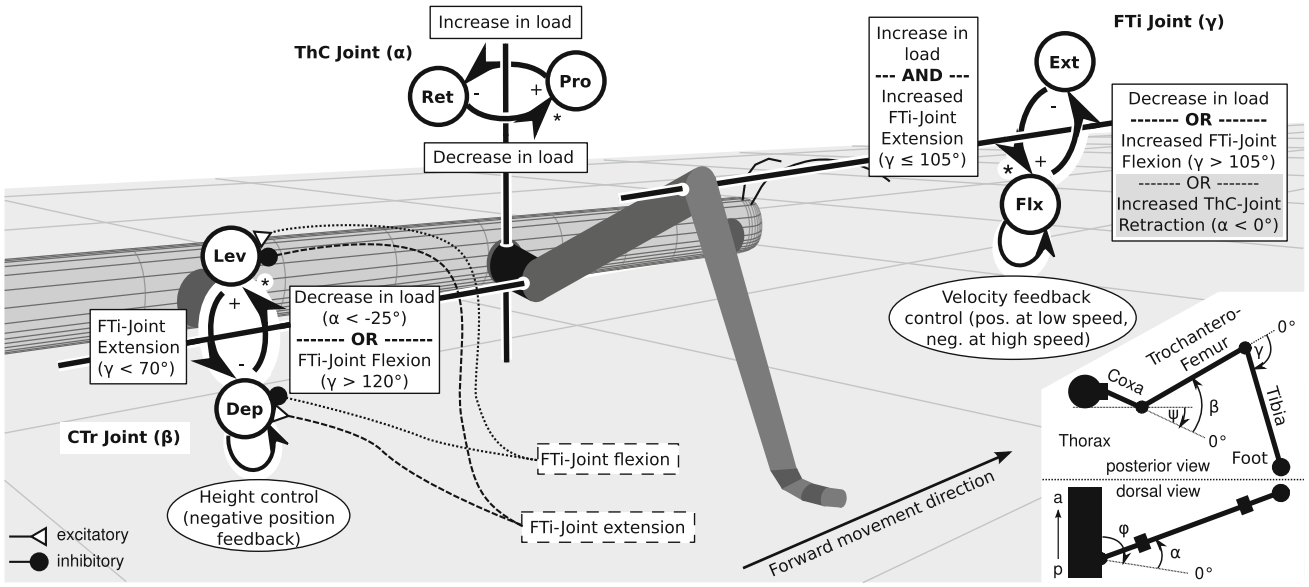

Fig. 1 Summary of rules given in Ekeberg et al. (2004) for each of the three main joints (joint axes are shown as *solid black lines*) of forward walking middle-legs: (1) State transition (timing) rules in joint controllers (*boxes* with *solid outline*), (2) Two types of magnitude control rules exist a. rules applying to one joint state (ellipse with solid outline) and b. rules that always apply (*boxes* with *dashed outline*). The sensor signals used by the corresponding control rules are given in *brackets*. Multiple conditions are connected via Boolean AND and OR. In case of conflicting state transition rules those marked with a * have priority. Optional conditions are shown with a *gray* background. The *inset* shows joint angle conventions (zero point and sign) and indicates joint axes ("leg plane") offsets ϕ and ψ (which are both zero for the robotic model) in a simplified way— for details see Cruse and Bartling (1995). *Pro* protraction, *Ret* retraction, *Lev* levation, *Dep* depression, Flx flexion, *Ext* extension, *a* anterior, and *p* posterior. The name of each joint angle is given in *Greek letters* in *brackets* after the joint name

decreased load, levation state is activated. In case of conflicting state transitions the one from depression to levation is given priority (not explicitly mentioned in the original publication, personal communication with authors). During depression phase sensory signals have an additional magnitude influence on the motor outputs, resulting in functional body height control: (1) CTr-joint position (β) is under negative feedback control and (2) FTi-joint position (γ) has an influence on CTr-joint motor activities such that body height changes due to FTi movement are reduced.

2.2 Neural networks

2.2.1 Neural network model

All neurons of the neuro-controllers were of the simple additive type with the standard sigmoidal transfer function σ:

$$\sigma(x) = \frac{1}{1+e^{-x}}, \quad x \in \mathbb{R}. \tag{1}$$

Sensor neurons were an exception because they used the unbounded identity function as transfer function. The discrete time dynamics of a recurrent neural network with m neurons was given by

$$o_k(t+1) = \sigma\left(\theta_k + \sum_{i=1}^{m} w_{ki}\, o_i(t)\right), \quad k = 1, \ldots, m \tag{2}$$

where o_k is the output of neuron k, θ_k denotes a bias term and w_{ki} is the synapse from i to k. Note that the discrete time dynamics incurred a fixed sequence of updates which here was an update of all neuron activations (the weighted sum of all inputs plus the bias) followed by an update of all neuron outputs. In turn, this meant for neural pathways that each additional synapse entailed a time delay of one time step. Network update was done with 100 Hz.

The Integrated Structure Evolution Environment (ISEE) software package (Ghazi-Zahedi 2008) was used to simulate neural networks (NN). It allowed to perform online structure and parameter manipulation, plotting, and logging to relate structure and parameter changes to changes in behavior.

2.2.2 Deriving modular neural network controllers

Based on Ekeberg et al. (2004) the rule-based controller (see Fig. 1) was implemented as a modular neural network. Required neuro-modules are described in detail hereafter and in Supplementary section S1 together with the implementation process that resulted in the final neuro-controllers.

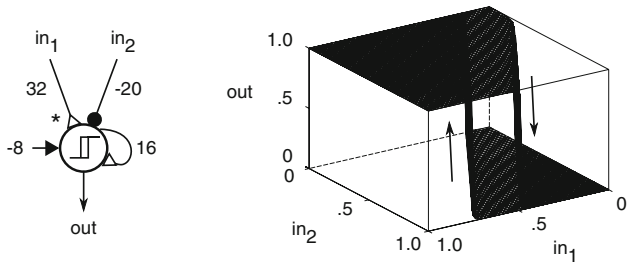

Fig. 2 Neuro-module serving as a switch with separate inputs for on (input 1) and off (input 2) switching. Using asymmetric input weights (unequal absolute input weights) one of the inputs can be given a higher priority. In the example shown input 1 (marked with a *) has priority over input 2 because it can switch on out independent of the state of input 2. Input 2, on the other hand, can only switch off out if input 1 is smaller ≈ 0.5. Note that each data point in the 3D plot was retrieved after 100 iterations to minimize transient effects

2.2.2.1 Switch module with separate and prioritized on and off triggers Bistable elements (see Supplementary section S1) as premotor elements ensured alternating activation of antagonist motor neurons. In the biological model two separate modules were used (at least in the CTr and FTi joints) for on and off switching of the respective bistable element. Depending on the parameters chosen and the sensory input, the two modules could have contradictory outputs, e.g., one commanding to switch from levation to depression and the other vice versa. In this case, the inputs were prioritized (see Fig. 2). The original implementation (Ekeberg et al. 2004) achieved the same with if-else-expressions, where the if case had highest priority.

2.2.2.2 Two-joint height control module As summarized in Ekeberg et al. (2004) (see also Fig. 1) two sensory influences affect the *magnitude* of the CTr motor neuron output but not directly the *timing*:

1. Intra-joint CTr negative position feedback is assumed to be a major component of height control in standing and walking animals (Cruse et al. 1993).
2. Inter-joint FTi → CTr influences exist that affect the Levator to Depressor activation ratio such that it is increased upon increased flexion and decreased upon increased extension (Bucher et al. 2003).

As depicted in Fig. 3, these magnitude influences were abstracted and combined in a height control servo module (cp. Supplementary section S1) for the CTr joint. We assumed that the coronal plane was parallel to the ground and that the leg segments trochanterofemur (femur) and Tibia had constant lengths. Then the height of the body above the ground was determined by the angular position of the two joints CTr (β plus offset ψ which is 0 for the robot) and FTi (γ) in combination with the segment lengths of Trochanterofemur (l_{Femur}) and Tibia (l_{Tibia}):

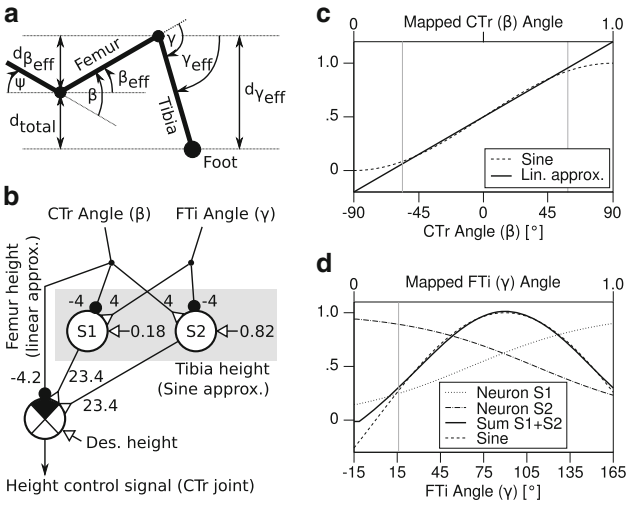

Fig. 3 **a** Body height depends on CTr (β) and FTi (γ) joint angles as well as on the CTr joint angle offset (ψ, which was 0 for the robot and varies for the different legs of the stick insect). **b** Proposed neuro-module to control the body height of the walking machine using the sum of the height influences of both joints as reference input and the desired height as control input to a comparator. Its output was used to control CTr motor neurons (parameters are given for the robotic model with $\psi = 0$). **c** CTr height influence was linearly approximated (shown here for $\psi = 0$), **d** FTi height influence with a two neuron sine approximator (shown here for $\beta_{\text{eff}} = 0$)

$$d_{\text{total}} = d_{\beta_{\text{eff}}} - d_{\gamma_{\text{eff}}} \quad (3)$$

$$= \sin(\beta - \psi) * l_{\text{Femur}} - \sin(\gamma - \beta + \psi) * l_{Ti} \quad (4)$$

The height influence of the CTr joint was linearly approximated, whereas the height influence of the FTi joint was given by a simple sine approximator; both were sufficiently accurate within the "normal" movement ranges (for comparison see, Cruse and Bartling 1995). CTr and FTi height influences were summed in a comparator neuron as controlled variable and subtracted from the desired height reference input. This resulted in a proportional height control servo. By multiplying all inputs to the comparator by the same factor and/or by multiplying the output synapse strength by a factor, the gain of the servo could be adjusted. Note that the ThC joint angle α and the axis offset ϕ had an influence if the axis offset ψ was non-zero as in the stick insect model. This influence was not taken into account here, and no neurobiological evidence for such an influence exists. In contrast, the Walknet implementation of a CTr height controller (Dürr et al. 2004) uses all three leg joint angles.

2.2.2.3 Complete controller Assembling the above-described neuro-modules to map the rules shown in Fig. 1 to a neural network and setting threshold parameters converted from those given in Ekeberg et al. (2004), we obtained the middle-leg forward walking controller depicted in Fig. 4: for all joints (proximal to distal from left to right) from top to

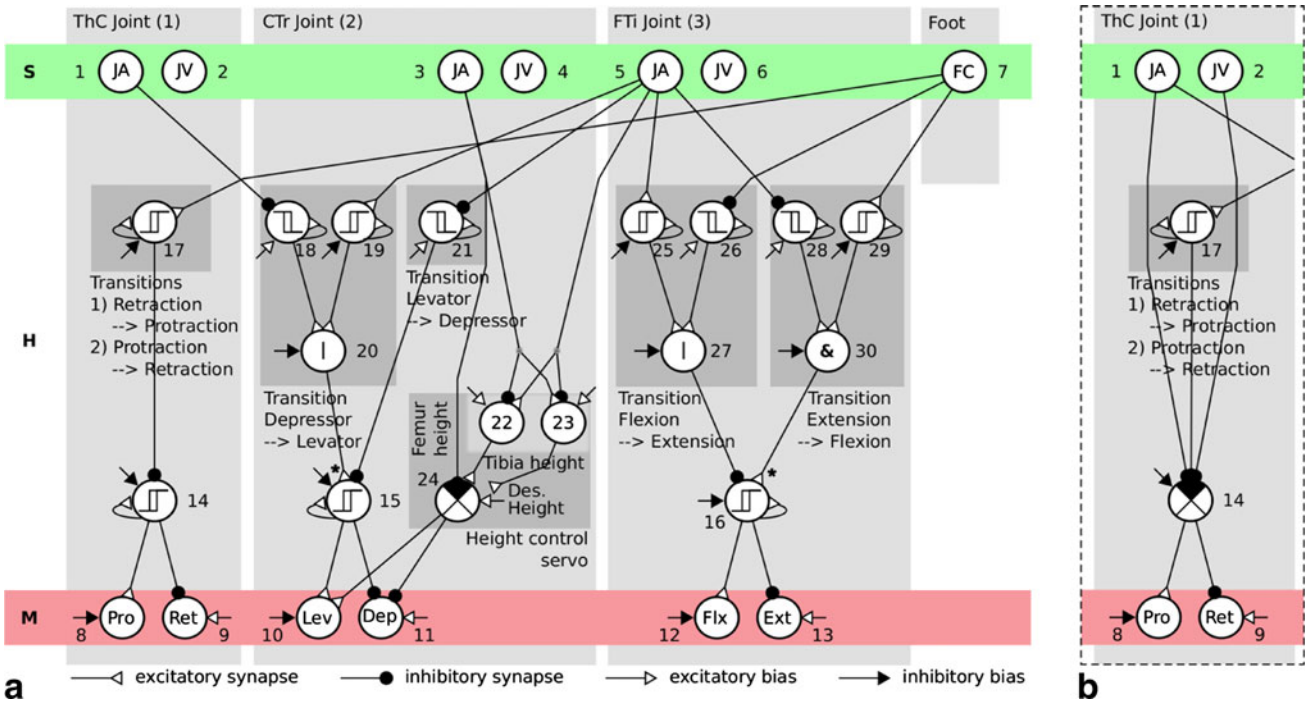

Fig. 4 **a** Complete controller transferred from Ekeberg et al. (2004) without modifications. Controller structure is applicable for middle- and front-legs. *S* sensor or input layer, *H* hidden layer, *M* motor or output layer, *JA* joint angle, *JV* joint velocity, and *FC* foot contact. Motor neuron abbreviations are given in Fig. 1. Neurons are numbered for easier reference from text. For a detailed description of the modules employed see Sect. 2.2.2 and electronic supplementary materials. **b** Alternative ThC joint control module extended by a neural servo to stabilize the joints working range. Restricted (sidewards) walking is achieved by setting the connection strength 17 → 14 to zero and by instead supplying the ThC neural servo with a fixed reference input via the bias of neuron 14 (not shown)

bottom proprioceptive intra- or inter-joint sensory signals were processed by threshold elements, combined with other sensor signals via Boolean elements and fed to bistable modules that functioned as premotor elements. Per joint one bistable premotor element antagonistically activated two motor neurons. In the CTr joint a parallel pathway from sensor to motor neurons existed that functioned as a height control module.

Neural threshold parameters were determined to meet two conflicting requirements: noise tolerance and fast switching. A broader hysteresis, i.e., a larger self-connection w_{self}, results in better noise tolerance but delays switching, and vice versa. Parameters $w_{\text{in}} = 32.0$ and $w_{\text{self}} = 5.0$ (see Supplementary Fig. S1) provided an optimal trade-off for both criteria within the synaptic weight limits of the network (see Sect. 2.2.1). The desired threshold was given as sensor neuron output value (SN_{thres}) which was mapped from the original sensor range (see Table 3). The bias value was then determined as

$$\text{bias} = -(w_{\text{in}} SN_{\text{thres}} + 0.5 w_{\text{self}}) \tag{5}$$

Additionally, the nonlinear threshold module behavior had to be taken into account, e.g., hysteresis effects introduced a shift of the switch threshold, depending on input signal frequency (see Supplementary Fig. S1). A bias adjust factor ($\text{bias}_{\text{adjust}}$) was experimentally determined as the difference of the bias calculated above and the bias at which the threshold unit output crossed 0.5 in the desired direction (see vertical lines in Supplementary Fig. S1) at a step cycle frequency of 0.75 Hz. This frequency was assumed to be the "standard" step frequency. An extended bias value calculation resulted:

$$\text{bias} = -(w_{\text{in}} SN_{\text{thres}} + 0.5 w_{\text{self}}) + bias_{\text{adjust}} \tag{6}$$

For example using $w_{\text{in}} = 32$ and $w_{\text{self}} = 5$ the correction factor would be approximately 3.2. Resulting neural parameters are given in Table 1 for angle thresholds. Foot contact threshold was set to half of the maximal activation of the foot contact sensor. Parameters are given for all leg types (front-, middle-, and hind-legs).

Parameters not prescribed by the neural rules nor explicitly given in the module descriptions are here called "free" parameters. They were tuned by hand (with the exception of the body support force simulations, see Sect. 2.4) while observing the resulting behavior. As subjective criteria stable and fast walking on flat ground were used. "Free" parameters were the premotor and height control to motor neuron synaptic weights, the motor neuron bias values and the reference inputs to the CTr height controller and the ThC servo controller.

Table 1 Transition rule switch parameters (joint angles) converted into neural parameters of sensor neuron (SN) and threshold neuron (TN)

Joint	Transition	Signal	Leg	Dir	Op	Thres (°)	Thres (SN out)	SN–TN	TN–TN	Bias adj.	TN bias
FTi	Flx → Ext	γ angle	ML	FW,S	$>$	105.0	0.667	32	5	3.2	−20.63
			FL	FW	$>$	95.0	0.611	32	5	3.2	−18.86
			HL	FW	–	–	–	–	–	–	–
	Ext → Flx	γ angle	ML	FW,S	$\leq$	105.0	0.667	−32	5	3.2	22.03
			FL	FW	$\leq$	95.0	0.611	−32	5	3.2	20.26
			HL	FW	–	–	–	–	–	–	–
CTr	Dep → Lev	α angle	ML	FW	$<$	−25.0	0.361	−32	5	3.2	12.26
			ML	S	–	–	–	–	–	–	–
			FL	FW	$<$	*10.0	0.556	−32	5	3.2	18.48
			HL	FW	$<$	−45.0	0.250	−32	5	3.2	8.70
		γ angle	ML	FW	$>$	120.0	0.750	32	5	3.2	−23.30
			ML	S	$>$	105.0	0.667	32	5	3.2	−20.63
			FL	FW	$>$	98.5	0.631	32	5	3.2	−19.48
			HL	FW	$<$	*55.0	0.389	−32	5	3.2	13.148
	Lev → Dep	α angle	ML,FL	FW,S	–	–	–	–	–	–	–
			HL	FW	$\geq$	5.0	0.528	32	5	3.2	−16.19
		γ angle	ML,FL	FW,S	$<$	70.0	0.472	−32	5	3.2	15,81
			HL	FW	$>$	*90.0	0.583	32	5	3.2	−17.96

Parameters are given for front-leg (FL), middle-leg (ML) and hind-leg (HL) as well as for forward walking (FW) and sidewards walking (S). For conversion formula see equation 6 and text. Entries marked with * were corrected from Ekeberg et al. (2004)

2.3 Physical simulator

Physical simulations of the walking machine Octavio and the stick insect model (see Supplementary section S3) were performed in an OpenDynamicsEngine (ODE Smith 2009)[2] based simulator called Yet Another Robot Simulator (YARS, Zahedi et al 2008). All relevant sensor and motor properties were implemented and each simulation, including walking machine and environment, was given in XML. It connected to the ISEE package, which simulated the NN, via User Datagram Protocol (UDP) communication. The physical simulation was updated with 200 Hz and every second step the NN update was triggered, sending sensor values and receiving new motor activations.

2.3.1 Single-leg simulator setup

Similar to the setup described in von Twickel and Pasemann (2007), the torso of the single-legged walking machine was mounted on a rail system that allowed for forward and backward movements (damping constant 10 $\frac{Ns}{m}$ to stop movements during stance in a reasonable time interval) and up- and downward movements (damping constant of only 1 $\frac{Ns}{m}$ because ventral hard stop was always active). Additionally, it had a lateral spring-damper (damping constant 200 $\frac{Ns}{m}$, spring constant 750 $\frac{N}{m}$) system to simulate lateral force influences of other legs (see Fig. 6). This allowed for small lateral movements similar to hexapod walking in stick insects (cp. Kindermann 2002). As an exception, the spring-damper system was replaced by a simple damper (damping constant 50 $\frac{Ns}{m}$) in sidewards walking simulations. Up-down and sidewards rails included force sensors to measure forces exerted by the leg.

The joint setup was similar to the one described in Ekeberg et al. (2004): each leg had three active hinge joints, namely Thorax-Coxa (ThC), Coxa-Trochanter (CTr), and Femur-Tibia (FTi). CTr and FTi joint axes were parallel to each other but different from the biological model the ThC joint axis was parallel to the dorso-ventral axis and orthogonal to the other two joint axes. Contrary to this and the biological model in Ekeberg et al. (2004), real stick insects have a ball and socket ThC joint. This may be viewed as a functional hinge joint where the axis of rotation changes during walking (Cruse and Bartling 1995). The lack of slanted rotation axes of the ThC joint potentially had implications for the control complexity and a significant effect on the ground reaction forces during stance.

2.3.2 Sensor and motor equipment

A summary of the sensor and motor equipment of the simulated robot is given in Table 2. Other sensors were exclusively used for analysis and as inputs for fitness functions during evolutionary parameter optimization (see below). Sensor-outputs were mapped onto sensor neuron (SN) inputs as specified in Table 3. For motor neurons no mapping was needed. To account for use on the hardware robot, artificial

[2] The ODE library is a game physics engine geared toward speed, a prerequisite for employing evolutionary algorithms. Successful transfers of complex controllers from simulations to real robots are used as the criterion of sufficient precision. For details please see the cited literature.

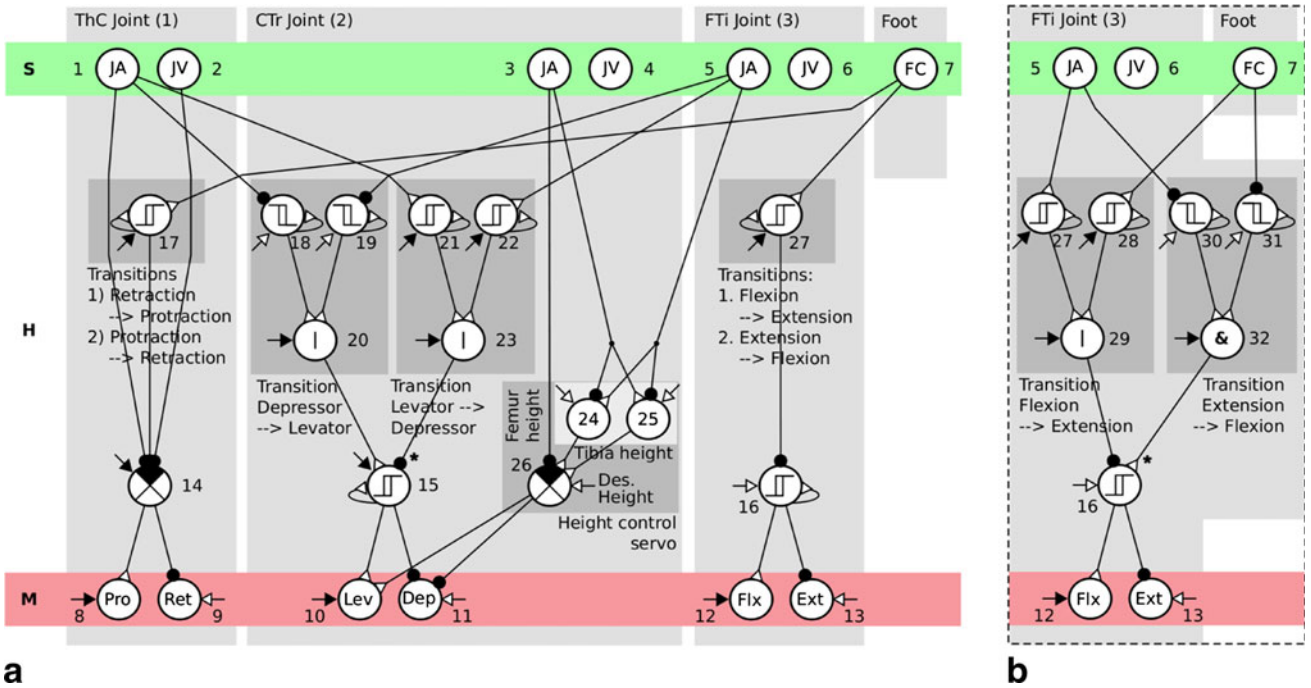

Fig. 5 **a** Hind-leg controller transferred from Ekeberg et al. (2004) with the same modified ThC joint control module as in middle- and front-leg controllers (see, Fig. 4b). CTr and FTi joint control modules have a different structure and partly different synapse signs. **b** Alternatively a FTi control module with the same structure as in middle- and front-legs but two inverted synapse signs is used. For abbreviations, see Fig. 4

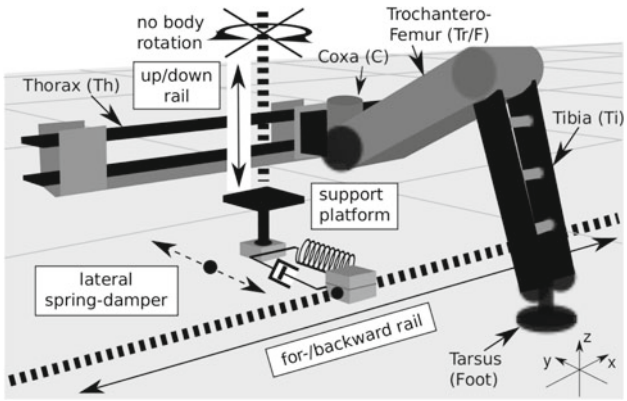

Fig. 6 Single-leg simulator setup with three degrees of freedom (DOF) rail setup. Forward- and backward movement was unlimited but slightly damped, sidewards movement was restricted by a stiff spring-damper system and up- and downward movement was damped, unlimited in upwards direction and limited in downwards direction by a support platform. No rotational movements was allowed. Additionally segment names of the walking machine are given. For joint names see Fig. 1

Table 2 Sensor and motor equipment of the walking machine

Segment/joint	Sensors	Motors
Body	(x, y, z) coordinate sensor*	
	Lateral torque to rail*	
	Dorso-ventral torque to rail*	
Joints ($3x$)	Angle	DC motor (Antagonistically controlled)
	Angular velocity	
	Torque*	
	Torque change*	
Foot	Contact	

Sensors marked with * were not used as controller inputs but only for analysis

noise of 1% (gaussian distribution) was added to all sensor- and 2% to all motor-signals used as inputs to, respectively, outputs from, the neural controller. All noise levels are given relative to the respective mapping ranges.

In contrast to the stick insect (Bässler 1983) each joint of the robot was driven by a single DC-motor. To approximate antagonistic control without requiring computationally costly controllers and to exploit the full motor dynamics the following general approach was chosen: the neural network gave antagonistic motor activations via two motor neurons (MNs), see Fig. 7. These were mapped on the four states (forward, backward, brake, and relax) of the motor H-Bridge[3] and the

[3] H-Bridges are electronic circuits with four operational modes allowing (1) to disconnect both motor terminals resulting in a free run or relaxed mode with minimal friction and no active torque, (2a, b) voltage to be applied in either direction to reverse motor polarity, (3) to shorten the motor terminals resulting in brake mode and effectively increasing rotational friction.

Table 3 Mapping of sensor values to sensor neuron outputs

Sensor	In min	In max	Out min	Out max
γ (angle)	−15°	165°	0.0	1.0
β (angle)	−90°	90°	0.0	1.0
α (angle)	−90°	90°	0.0	1.0
FC (foot contact)	No contact	Contact	0.0	1.6
α', β', γ' (velocity)	−300°/s	300°/s	0.0	1.0
Joint torques	−10 N	10 N	0.0	1.0
(Joint torque)′	−200 N/s	200 N/s	0.0	1.0

pulse width (PW) of the pulse width modulation (PWM)[4] control signal. The mapping was performed as follows:

1. Low activations ($\leq$ 0.1) in both antagonistic MNs resulted in a *relaxed* motor (consuming no energy, producing no active torque).
2. A strong absolute ratio in favor of one MN

$$\left|\frac{\mathrm{MN1}-\mathrm{MN2}}{\mathrm{MN1}+\mathrm{MN2}}\right| \geq 0.15 \tag{7}$$

   resulted in a *forward* (positive ratio), respectively, *backward* (negative ratio) movement. The larger the absolute difference (|MN1−MN2|) the higher the power output of the motor (resulting in higher torques and/or velocities, depending on the environment).
3. Otherwise approximately equal MN activations resulted in the motor *brake* mode and therefore increased effective joint friction without consuming energy. The effective brake strength was set proportional to the sum of motor neuron activations ((MN1 + MN2)/2).

The motor activation and environmental conditions (external torques) determined the joint movement. This was registered by sensors and fed back into the neural network, together with other sensory information.

2.3.3 Technical data of the simulated robot

In supplementary Table S1, technical details of the simulated robot and corresponding stick insect data, along with relevant literature, are given. Additionally, scaling ratios comparing robot and stick insect are provided.

2.4 Evolutionary parameter optimization

In some simulation experiments parameters of front-, middle-, and hind-leg controllers were separately optimized with an evolutionary algorithm. Here, resulting controllers were compared with respect to their ability to support the body weight during stance phase of forward walking. This was assumed to be indispensable for realizing hexapod walking behavior.

[4] PWM control allows to supply intermediate amounts of power by varying the ratio of discretely switching on and off the power supply.

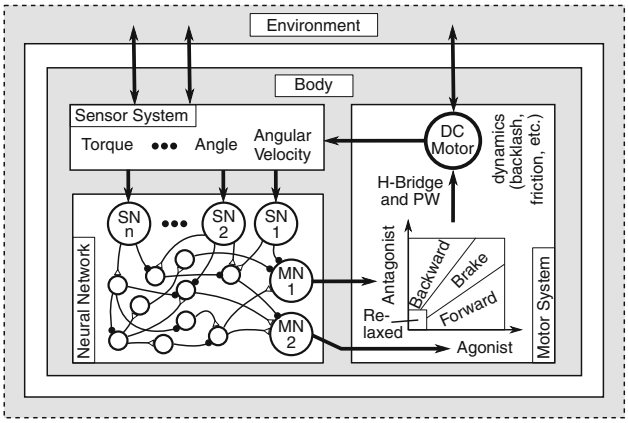

Fig. 7 Joint control with antagonist motor activation (see text for details)

2.4.1 Evaluation

2.4.1.1 Terminate try signals Evaluations were stopped when joint angles exceeded ranges roughly corresponding to those given in Cruse and Bartling (1995) for free walking animals. Hereby maximum angular ranges for CTr (−25–50 °) and FTi (20–125 °) were assumed to be equal in all leg types, and angular ranges for ThC joints differed between leg types (Fl: −10–60 °, ML: −50–40 °, HL: −60–10 °). Therefore, no explicit trajectories were prescribed but rather desired joint angular ranges.

2.4.1.2 Fitness function Total fitness was the sum over all single step fitness values whereby the total number of steps could differ if terminate try conditions were used (s.a.). The total fitness for n time steps was calculated by taking into account the distance covered since the last step in forward direction (Δw) and the body support force (f) as follows:

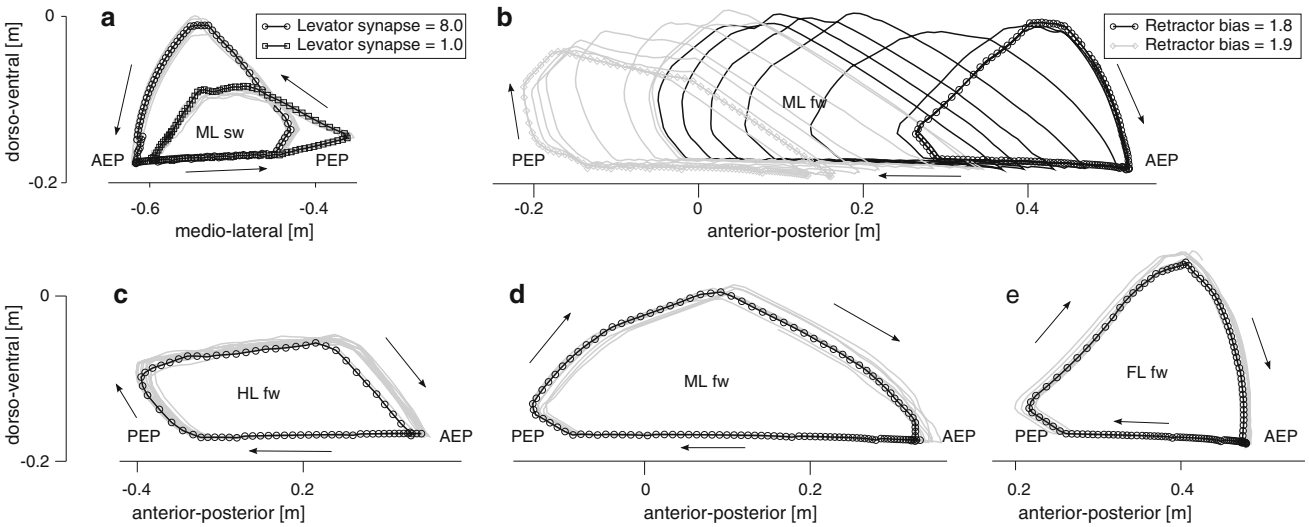

Fig. 8 Foot trajectories of stepping (in *brackets* figures with respective controller structure and supplementary section with respective parameter set are given): **a** restricted (sidewards) in middle-leg (Fig. 4b, S4.1), **b** forward in middle-leg (Fig. 4a, S4.2), **c** forward in hind-leg (Fig. 5a, S4.5), **d** forward in middle-leg (Fig. 4b, S4.3), and **e** forward in front-leg (Fig. 4b, S4.4). Medio-lateral distances are relative to the midline of the torso, anterior-posterior distances relative to the coxa position of the respective leg. Each trajectory shows a 10 s run, and for exactly one step cycle individual data points for every simulation time step are shown as *black* markers on a *black line*, the rest in *gray*. This is slightly different in sub-figure **b** where one 10 s trajectory is shown as a *black line* and the other as a *gray line* to allow distinction between both in overlapping regions. For both trajectories the last step cycle of the 10 s periods has individual markers for each time step. *Arrows* indicate the direction of foot movement and anterior and posterior extreme positions (AEP and PEP) are labeled. In each of (**a**, **b**) two trajectories are plotted to show the influence of changing a single parameter (indicated in *inset* legend): Changing the strength of the levator synapse in the restricted middle-leg controller resulted in changing trajectory height (**a**). Changing the retractor bias in the unrestricted and unmodified middle-leg controller resulted in the trajectory either drifting anterior or posterior (for details see text)

$$Fitness = \sum_{i=0}^{n} \Delta w_i \; f_i \tag{8}$$

The body support force term could take values between 0 (no body support provided by leg, full weight support by rail suspension) and 1 (full body support by leg, no weight support by rail suspension).

2.4.2 Evolutionary algorithm

As evolutionary algorithm the evolution of neural systems by stochastic synthesis (ENS^3) was employed as described in Hülse et al. (2004). ENS^3 is an implementation of a variation–evaluation–selection loop operating on a population of neuro-modules. All structure evolution parameters were disabled, allowing only synapse strength and bias strength changes during evolution. Evolution was seeded with the front-, middle-, and hind-leg controllers described in the Sect. 3. Parameters of the height control module were fixed because of its fragile parameter set. In the "restricted" case only motor and premotor neuron bias values as well as synapses to motor neurons were allowed to change. In the "unrestricted" case all input and output synapses of the height control module were allowed to change, as well as all other parameters of the networks. Maximum evaluation time was set to 2,000 steps (corresponding to 20 s), population size to 100, and evolution was run for 1,000 generations. For each leg-type evolution was repeated five times, and the best performing network of the last generation of each evolution was taken as a basis for analysis.

3 Results

3.1 Middle-leg walking

3.1.1 Restricted (sidewards) middle-leg walking

In biological experiments the term "restricted preparation" denotes a fixated ThC joint resulting in solely CTr and FTi joints moving the leg in a vertical plane. This was the only experiment where sufficient neural data was available to fully describe a functional walking controller and therefore we performed a corresponding simulation first. In the simulation conducted here the ThC joint was not mechanically fixated but rather neurally by means of a stiff neural servo controller with constant reference input. The restricted middle-leg controller shown in Fig. 4b is a modified version of the controller shown in Fig. 4a that, in addition to the neural ThC servo, has all sensori-motor influences between ThC

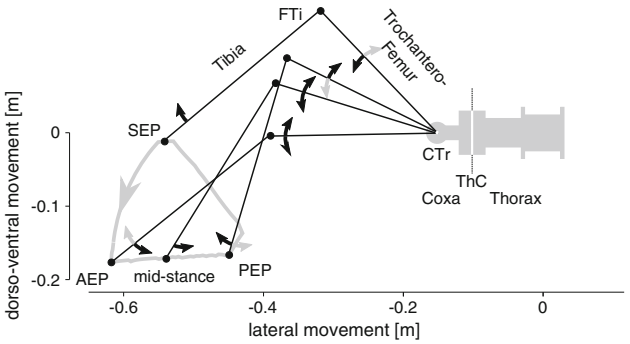

Fig. 9 Anterior view of a restricted middle-leg swing–stance cycle. Joint movement directions are indicated as *black arrows* at the next distal segment, and, if a transition took place, the old movement direction is additionally given in *gray*. Note that during stance the CTr height controller was active, therefore, both CTr movement directions occurred (for details see text)

and other joints removed. Neural network parameters were translated from the Ekeberg controller as described above and remaining parameters, especially synapse strengths between the bistable elements and the motor neurons, were tuned by hand. Simulation results for parameters given in Supplementary section S4 are depicted in Fig. 8a (foot trajectory) and Fig. 10a (time plot of important simulation parameters like sensor and motor activations). Peak sidewards torso velocity during a step was $v_{\max} = 0.47$ m/s.

A simple swing–stance cycle is depicted in Fig. 9: During swing phase the FTi joint was in extensor state and the CTr joint in levator state. A progressed extension of the FTi joint caused the CTr joint to switch from levation to depression state at the swing extreme position (SEP). Subsequent ground contact at AEP resulted in the FTi joint to change extension to flexion state, resulting in the stance phase where FTi was in flexion and CTr in depression state. During stance phase the CTr joint displayed its height control mechanism. Progressed flexion in FTi caused FTi and CTr to change states at the PEP resulting in the swing phase, and the swing–stance cycle started over again. Overall, restricted middle-leg controller translation to a neural network and test on the simulated robot worked well. One has to keep in mind that by changing synapse strengths to the motor neurons behavior could be easily modified. Additional to the example given above (trajectory height), e.g., a slow down of stepping could be achieved via a decrease in flexor synapse strength.

Kinematics of restricted stepping was similar to that found in von Uckermann and Büschges (2009) and Fischer et al. (2001) but differed in details. In von Uckermann and Büschges (2009), (1) the absolute movement of the CTr joint is more limited and (2) the CTr joint angle shows two depression maxima during stance phase. Two adaptations allowed to reproduce results of the biological experiments: (1) Tuning the neural parameters, especially levator synapse and bias values, the initially flat trajectory could be reproduced (see Fig. 8a) and (2) raising the body height in the simulator setup, such that it matched that of the experiment in von Uckermann and Büschges (2009) (trochanterofemur parallel to ground and tibia at an right angle to the ground allow for ground contact), the two depression peaks during stance could be reproduced because CTr then had to depress during end of stance to continue ground contact (data not shown).

3.1.2 Forward middle-leg walking

Without the restriction of fixating the ThC joint, the leg was expected to be able to walk forward by employing all three DOFs. The controller structure shown in Fig. 4a corresponds to the original Ekeberg controller and parameters were calculated as explained above. As an exception, premotor- to motor neuron synapse strengths were tuned by hand (cp. Sect. 2.2.2, paragraph "Complete controller"). Using this approach, no robust parameter set could be found that resulted in stable trajectories in the desired range. As shown in Fig. 8b for the parameter set given in Supplementary section S4.2 it was difficult to stabilize the working range of the ThC joint—slight parameter changes resulted in ThC trajectories either drifting anterior or posterior. In anterior and posterior positions finally stable trajectories would result but not in the desired working range for middle-legs. By performing very precise parameter tuning, trajectories in the desired range could be achieved for a short time but upon minor external disturbances they again drifted away.

3.1.2.1 Extension of middle-leg forward controller The controller in Fig. 4a was extended by a neural servo controller of the ThC joint to stabilize its working range, and the resulting controller structure is shown in Fig. 4b. Parameters not determined by the rules given above were tuned by hand to achieve stable forward walking. Simulation results for the parameter set given in Supplementary section S4.3 are depicted in Fig. 8d (foot trajectory) and Fig. 10b (time plot of important simulation parameters). Peak forward torso velocity during a step was $v_{\max} = 1.03$ m/s. Again tuning parameters resulted in modified behaviors, e.g., decreasing retractor and/or flexor synapse strength resulted in slower walking (see Sect. 3.1.3 for details), ThC comparator bias could shift AEP and PEP, and all parameter influences given for the restricted middle-leg controller also held for this one.

Alternative extensions to the original ThC joint controller module of the middle leg, all based on intra-joint sensorimotor feedback, have been tested, e.g., position-dependent agonist and antagonist output limitation, corresponding to simple linear muscle models. These solutions, although not shown here, also worked fine in stabilizing the ThC working range.

Kinematics of forward stepping was found to be similar to the stick insect (cp., e.g., Fig. 3 in Cruse and Bartling 1995) with one exception: Fig. 10b shows that with the parameters chosen the FTi joint was in flexion state throughout the stance cycle. A biphasic flexion-extension movement during stance, as frequently seen in the stick insect (Cruse and Bartling 1995), could be achieved by modifying parameters for two threshold units (data not shown): first, the threshold for FTi flexion leading to a transition from depression to levation (neuron 19) needed to be set so low that it was practically disabled and the ThC retraction threshold (neuron 18) led to the transition to levation. Second, the threshold for FTi flexion leading to a transition from flexion to extension (neuron 25) needed to be set so high that extension was triggered by flexion movements normally achieved not only during mid-stance and but also later by the loss of foot contact (neuron 26). Since smooth movements only resulted if the flexion-extension transition took place while ThC(α)-joint angle was $\approx 90°$ resulting controllers showed to be very sensitive to changes in environmental conditions. Adding a neural ThC angle influence on flexion-extension transitions allowed robust stepping under different environmental conditions, together with the biphasic FTi movement during stance.

3.1.3 Velocity control

In Fig. 12, details of the velocity control are given: locomotor speed (due to the single leg simulations it was measured as average velocity during stance) could be varied between 0.26 and 0.75 m/s by exclusively changing retractor and flexor bias parameters. 11 sets of both parameters were manually chosen to cover the range between the slow and the fast locomotor speeds (for parameter sets with corresponding velocities see Supplementary section S4.3). Up to a locomotor speed of $\approx$ 0.6 m/s velocity increase was mainly achieved by a decrease in step cycle duration. While swing phase duration was approximately constant across all velocities a decrease in stance duration was responsible for the decrease in total step duration. The increase in stance velocity in turn was caused by an increase in flexion and retraction velocity (data not shown). With the parameters chosen the flexion velocity increase had a larger influence than the retractor velocity increase resulting in the side effect of a slightly decreased step length: since levation was triggered above a flexion threshold (neuron 19) increased flexion velocity led to a slightly earlier levation during stance. For velocity increases above $\approx$ 0.6 m/s an increase in support length (distance body travels during contact phase, Halbertsma 1983) was observed while both stance and swing phase duration slightly decreased. For the parameter sets chosen stance velocity increase was predominantly due to an increase in retraction velocity. In this situation, the switch from depressor to levator activity was first triggered by the retraction signal (neuron 18) and not the flexion signal (neuron 19). This resulted in an extended, i.e., more retracted, step. Therefore, the FTi angle at PEP was not as flexed as during slower movements, and the angular range to reach the extension inducing depression was smaller. This led to shorter swing phases. The bistability of the ThC comparator input (17 $\rightarrow$ 14), together with the extended retraction, led to a larger error signal in the ThC servo (neuron 14) during early swing and therefore to a higher protraction velocity.

3.1.4 Test of controllers under different perturbing conditions

Leg controllers were tested with regard to their robustness under perturbing conditions. In Fig. 13, results are shown for the middle-leg, using the same neural structure (Fig. 4b) and neural parameter set (Supplementary section S4.3) as above. The controller proved to be robust against substantial changes in all tested conditions:

3.1.4.1 Ground height variations In Fig. 13a, ground height was varied, alternating every 0.8 m between low and high steps. Heights were randomly chosen in the ranges [0.05; 0.27] m and [0.15; 0.37] m below torso support height. Ground height variations were tolerated without disrupting the walking behavior. During stance phase the foot was more medial for low steps and more distal for high steps (see, Fig. 13f). During some steps the swing trajectory appeared to be especially flat, during others especially high. Therefore, swing data of the same simulation but for an extended number of swings (40) was plotted in different formats in Fig. 14: first of all in the overlaid swing trajectories (Fig. 14a) a correlation of low and anterior PEPs, on the one hand, and high and posterior PEPs, on the other hand, was noted. In contrast, x and z components of AEPs were less correlated because the x component was, especially for low AEPs, less variable. Therefore, also the anterior-posterior swing length was positively correlated with the PEP height, i.e., high PEPs resulted in longer swings than lower PEPs. With some exceptions (see below) PEP–SEP slopes continuously decreased with increasing PEP height resulting in a negative correlation of dorsal-ventral swing amplitude ($SEP_z - PEP_z$) and PEP height, i.e., swing amplitude decreased with increasing PEP height (Fig. 14b).

As mentioned above, two types of deviations occurred from the average swing behavior: for very high PEPs dorsal-ventral swing amplitudes could be much larger than for slightly lower PEPs, and for very low PEPs dorsal-ventral swing amplitudes could be much lower than for slightly higher PEPs. Dorsal-ventral swing amplitude depended on mainly two components: tarsus levation time and levation velocity. Levation time was dependent on the state of the CTr and FTi premotor neurons which were in turn dependent on

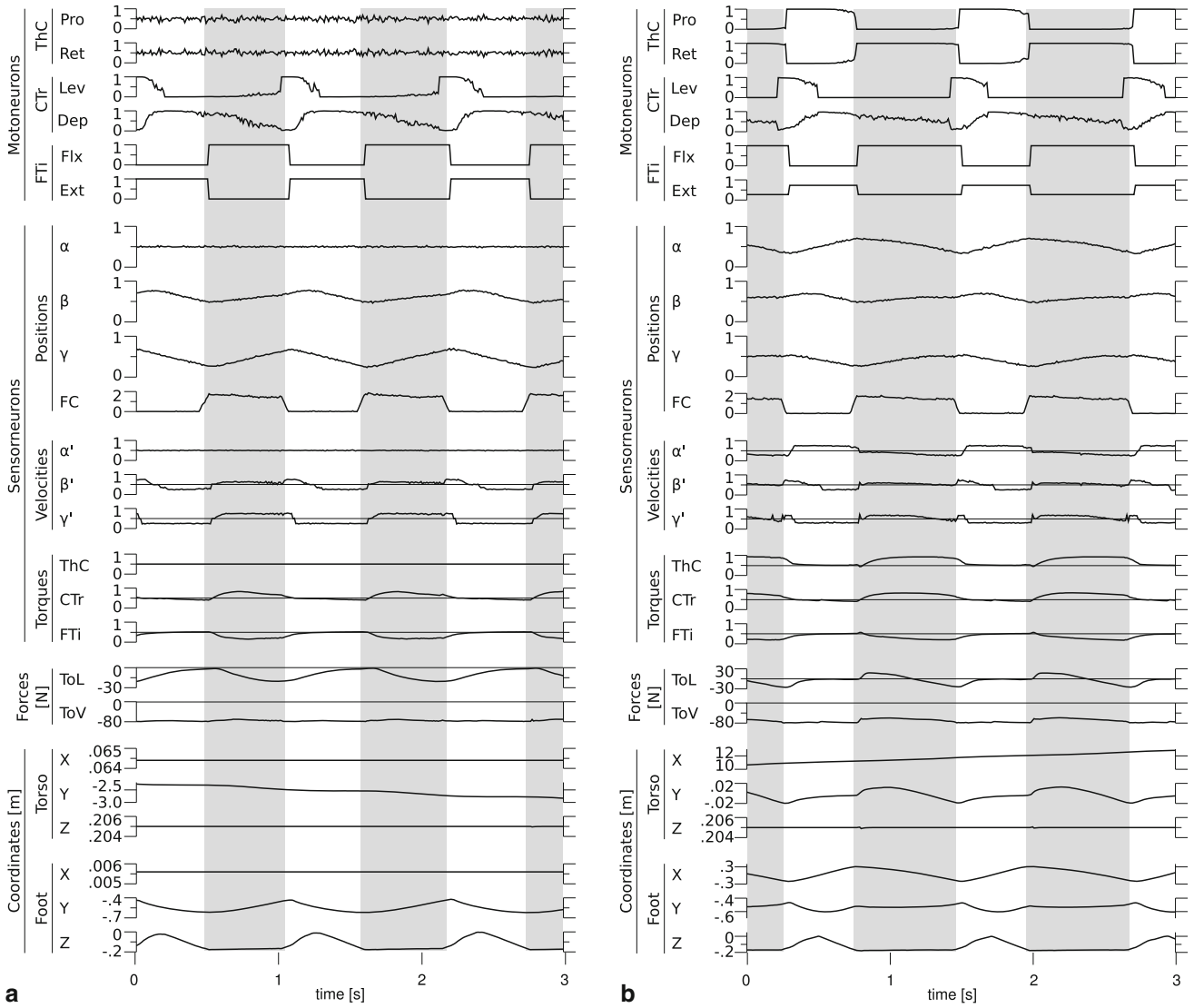

Fig. 10 Various data of **a** restricted (sidewards) and **b** forward walking in a single middle-leg. *Gray areas* indicate stance phase. Velocities, torques, and forces are shown together with a base line indicating zero velocity, torque, or force. For abbreviations see Fig. 1 and 4 and additionally: *FC* foot contact, *ToL* torso lateral, *ToV* Torso Vertical

the antagonistically acting state transition modules. Levation velocity was mainly dependent on the CTr height control module. In the "normal" cases, where the negative swing height to PEP_z correlation held, levation time moderately increased with PEP height (0.24s with PEP_z of −0.29 m and 0.29 s with PEP_z of −0.06 m, see Fig. 14c). As shown in the same sub-figure, this levation time increase was due to the FTi angle at PEP because the further the FTi joint was flexed, the longer it took for it to reach the extension threshold during swing triggering depression (neuron 21 in Fig. 4). Therefore, a higher levation velocity for lower PEPs had to compensate for the shorter levation times and additionally had to cause the differences in swing height amplitude. In Fig. 14d, a strongly decreasing average CTr angular velocity between PEP and SEP is shown for increasing PEP heights supporting this hypothesis. For one extreme outlier the very low average angular velocity of CTr (18°/s at −0.29 m PEP_z) was responsible for the low swing height. It was caused by a swing phase where the CTr joint was not switched to swing phase but rather its height controller was initiating a levation in response to FTi flexion. This led to ground contact loss and in turn to a switch from flexion to extension in the FTi joint and a switch from retraction to protraction in the TC joint. The extension quickly triggered a depression via the height controller. For the remaining outliers the time from PEP to SEP and therefore the FTi-angle at PEP was identified as the cause: for very low PEPs FTi was less flexed in three cases (depression–levation switch caused by TC angle retraction

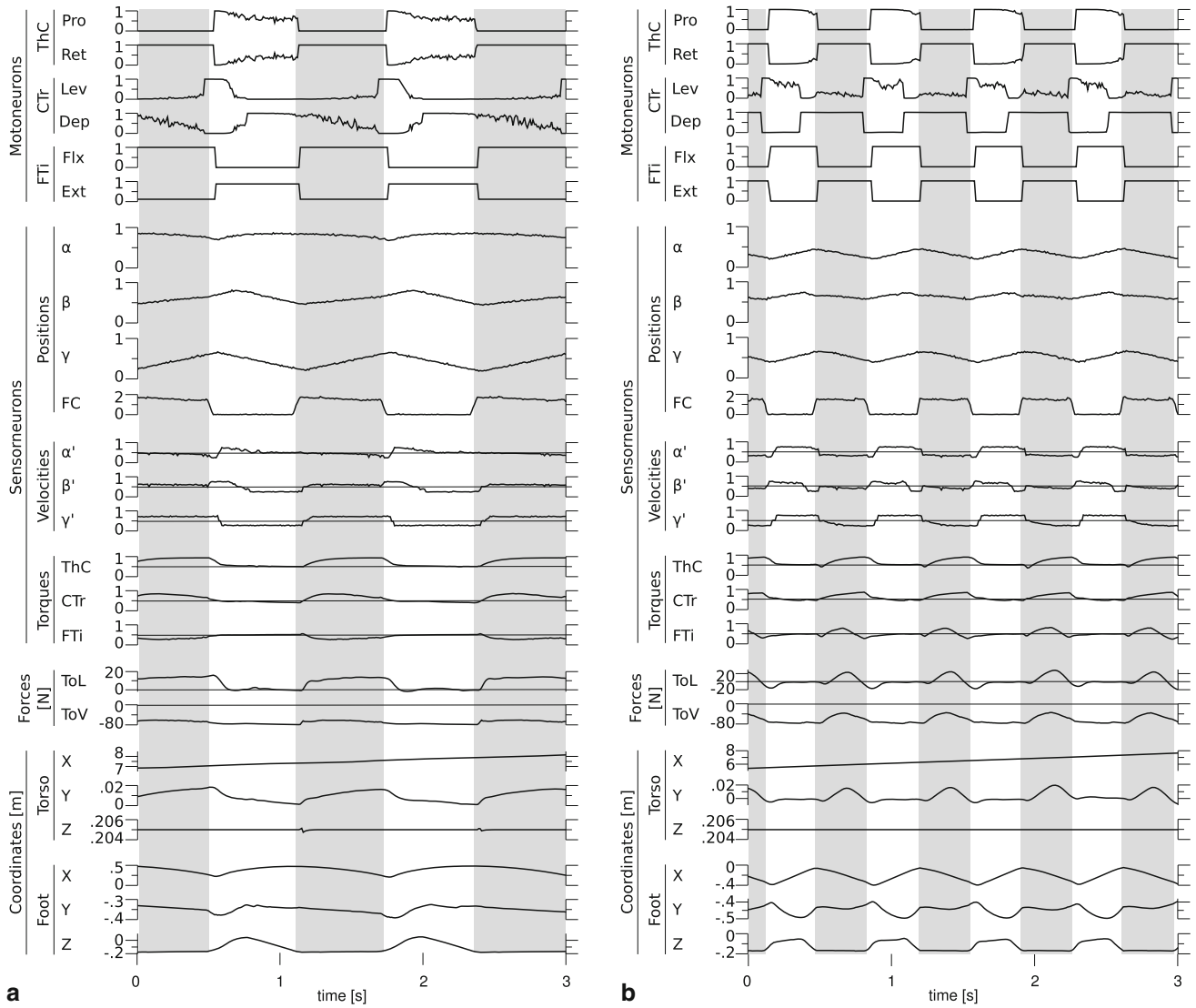

Fig. 11 Various data of forward walking in single **a** front- and **b** hind-legs. For abbreviations and further explanations see Fig. 10 and text

threshold) leading to a shorter extension period and therefore a faster switch from levation to depression. For very high PEPs FTi was flexed stronger in four cases leading to a longer extension and therefore to a longer levation time.

3.1.4.2 Lateral "kicks" In Fig. 13b, lateral forces with a magnitude (80 N) larger than a third of the robots weight ($\approx$ 216 N/3, corresponding to the weight that one leg had to support in tripod gait) were applied alternatingly from both sides with pauses in between. Due to the lateral spring-damper suspension system perturbation forces would lead to movements during force on- and offset. During stance lateral torso movements were compensated by the leg joints (especially the FTI joint) and not by a sliding foot. Forces did not disrupt the walking behavior and only had a minor influence on swing trajectories despite the obvious lateral shifts during lateral force application. In Fig. 13f, it is shown that during stance phase lateral directed forces decreased the torso-foot distance whereas medial-directed forces increased it. Larger perturbation forces (data not shown) could lead to instability in the sense that beyond FTi extension the foot was dragged across the ground, or that beyond FTi flexion the foot was tilted inwards.

3.1.4.3 Simulated up- and downhill walking In Fig. 13c, up- and downhill walking was simulated by an application of varying forces at angles of 45° from either anterior-dorsal ("uphill") or posterior-ventral ("downhill"). Forces corresponded to approximately 4, 8, and 12% of body weight and, if assuming other assisting legs as during tripod or wave gait in a hexapod, the per leg forces were proportionally higher (3–5 times, i.e., 12–36% in tripod and 20–60% in wave gait). Under these perturbing conditions the leg controller showed robust walking behavior and, together

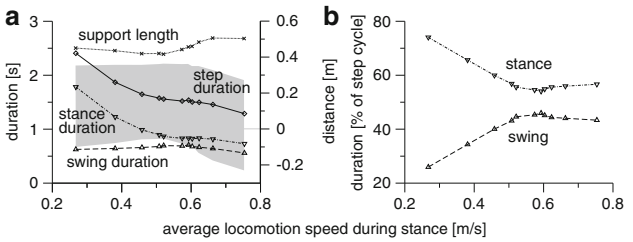

Fig. 12 Relative changes in the duration of swing and stance phases of the step cycle as well as changes in the support length at different speeds of forward locomotion in the middle leg. Locomotion speed was controlled by changing retractor and flexor motor neuron (neurons 9 and 12, see Fig. 4) bias values. Data is displayed for 11 bias parameter sets (given in the Supplementary section S4.3), each averaged across five steps. In **a** absolute step cycle, swing and stance durations and the support length, together with anterior-posterior tarsus range relative to the coxa during stance (*gray area*), are given whereas in **b** swing and stance phase duration relative to the total step cycle duration is given. Locomotor speed was calculated by averaging torso velocity during stance phases (see text for details)

with the bio-mechanical system, a velocity adaptation. In Fig. 13g, data of separate simulation runs for each external force level are shown: "uphill" locomotion speed was reduced and "downhill" locomotion speed increased. The velocity adaptation was mainly due to a step duration variation, which was in turn due to a stance duration variation, and to a small extent due to support length variations. Note that forces were applied independently of stance or swing phase and therefore the variation in global swing amplitude did not correspond to the step length relative to the torso (see, Fig. 13f).

3.1.4.4 Noise on sensor and motor neurons In Fig. 13d and e, noise of varying levels was applied to all motor neuron outputs (d) all sensor-neuron inputs (e) at the same time. On the one hand, noise levels on motor neuron outputs could be increased to $\approx 40\%$ without disrupting basic stepping. With increasing noise levels swing trajectories became smaller in height and length as well as slightly more jittery and showed increasing lateral deviations (cp. Fig. 13f). Beyond $\approx$40–45% noise level no regular walking behavior could be observed any more. On the other hand, noise levels on sensor-neuron inputs could only be increased to $\approx$15% before becoming disruptive. Both increased sensor and motor noise additionally shifted the foot position during stance further distal (see, Fig. 13f).

3.2 Test of controllers in front- and hind-legs

In Ekeberg et al. (2004), the middle-leg controller structure was also tested on front- and hind-legs. For the front-leg only parameters of the original middle-leg controller had to be changed because kinematics does change little when compared to the middle-legs: ThC joints of front-legs are on average more protracted during stepping. Here the parameters given in Ekeberg et al. (2004) were directly translated into neural parameters and applied to the original middle-leg controller structure shown in Fig. 4. The same problem of stabilizing the ThC working range appeared as initially in the middle-leg, so a neural ThC servo was included. This resulted in the same controller structure as finally used for the middle-leg (see Fig. 4b). Employing this structure and tuning the "free" parameters resulted in stable forward walking in the desired working range. Simulation results for neural network parameters given in Supplementary section S4.4 are shown in Fig. 8e (foot trajectory) and Fig. 11a (time plot of important simulation parameters). Peak forward torso velocity during a step was $v_{\max} = 0.79$ m/s. By changing parameters, front-leg walking kinematics could be changed in several ways. In addition to the behavioral flexibility listed for the middle-leg, e.g., "anterior sidewards" stepping (i.e., forward walking largely without ThC joint contribution) could be achieved by either changing ThC comparator reference input or protractor and retractor synapse strength.

In contrast to the front-leg controller the structure of the middle-leg controller had to be modified in Ekeberg et al. (2004) to make it work as a hind-leg controller. The kinematics of the hind-leg differs significantly, especially the phase relation of the FTi joint relative to the other two joints, with the extensor being active during stance phase and the flexor during swing phase. In addition to the modifications by Ekeberg et al. (2004), we had to introduce the neural ThC servo to stabilize the ThC working range, analogous to front- and middle-legs. The resulting structure is shown in Fig. 5. Parameter tuning by hand proved to be more difficult than for front- and middle-legs. Therefore, a prioritizing switch module (see Fig. 2) was included in the CTr joint controller and resulted in robust walking behavior under standard conditions. Simulation results for the parameter set given in Supplementary section S4.5 are shown in Fig. 8c (foot trajectory) and Fig. 11b (time plot of important simulation parameters). Peak forward torso velocity during a step was $v_{\max} = 1.05$ m/s. As in the other leg controllers behavior could be modified by changing neural parameters but due to the different kinematics of the hind-leg (s.a.) differences in behavior control existed: for instance a combination of depressor and extensor synapse strength determined velocity during stance phase (and therefore step period), a combination of flexor and levator synapse strength determined swing velocity and duration (data not shown).

Under perturbing conditions, like changing ground height (data not shown, cp. Sect. 3.1.4 for middle-legs), the performance of the hind-leg controller was not robust in all situations despite new parameter tuning. This was because the FTi joint was prone to flex too far, and subsequently the controller was "stuck" because the FTi joint would only switch

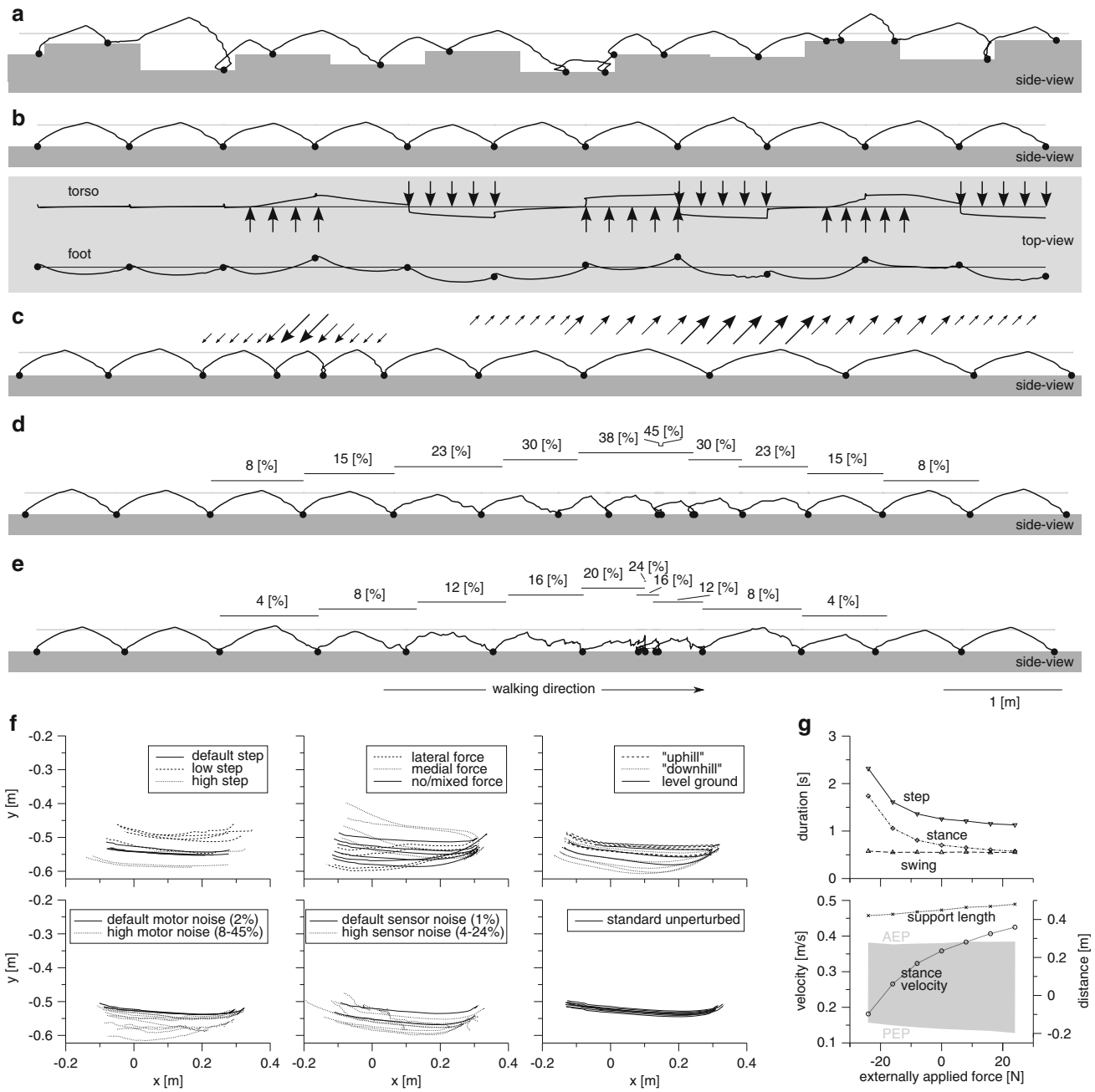

Fig. 13 Middle-leg walking forward under different perturbing conditions. Foot trajectories in world coordinates are shown as a *black line*, foot contact with ground as *black dots* and ground as *gray area*. Viewpoints are indicated in figure. **a** Ground height changes with fixed body suspension height (*straight gray line*). Total time period was ≈20 s. **b** Sidewards forces of 80 N were applied to torso whenever arrows are shown with direction of the arrows (note that torso was fixed to a lateral spring-damper system so it had an equilibrium position shown by thin line, see Sect. 2 for details). Periods of force application were randomly chosen between 0.9 and 1.1 s. Total time period was ≈15 s. **c** Forces with magnitudes 8, 16, and 24 N were applied at an angle of 45° from anterior-dorsal and posterior-ventral to simulate up- and downhill walking. *Arrows* show when forces were active, in which direction and with which strength. Periods of force application were randomly chosen between 0.9 and 1.1 s for all forces. Total time period was ≈14 s. **d** Gaussian noise on motor neuron output. Magnitudes of noise application are indicated in the figure. Periods of noise application were randomly chosen between 1.4 and 1.6 s. Total time period was ≈19 s. **e** Gaussian noise on sensor neuron input. Magnitudes of noise application are indicated in the figure. Periods of noise application were randomly chosen between 1.4 and 1.6 s. Total time period was ≈20 s. **f** For all perturbing conditions above (**a**–**f**) and the reference flat ground condition the dorsal view of the foot stance trajectories relative to the middle-leg coxa is given (for details see text). **g** For the simulated up- and downhill perturbing condition **(c)** average stance velocity and other important step cycle parameters (s.a. Fig. 12) are given for the external force levels listed above (each data point was averaged from seven consecutive steps)

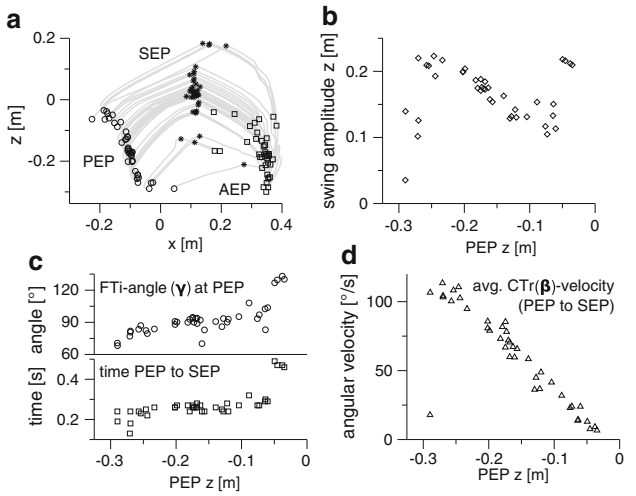

Fig. 14 Detailed swing trajectory data from 40 consecutive steps, taken in an environment with varying ground to torso suspension height (see Fig. 13a): **a** Lateral view of swing trajectories (*gray*) with markers for posterior-, swing-, and anterior-extreme positions (PEP, SEP, and AEP). **b** Swing height ($SEP_z - PEP_z$) versus PEP height. **c** FTi angle (γ) at PEP and PEP to SEP duration versus PEP height. **d** Average CTr (β) angular velocity in PEP–SEP interval versus PEP height. Note that four swings from low and four swings from high ground deviated from the general pattern (see text for details)

to extension upon ground contact, but ground contact without extension was not possible any more. To obtain a more robust hind-leg controller two alternatives were tested (data not shown): (1) using a neural servo controller in the FTi joint analogous to the ThC joint, (2) using the FTi joint controller structure found in the front- and middle-legs (see Fig. 5b and Supplementary section S4.6 for controller parameters). Both solutions led to an increased stability in the FTi joint.

3.3 Test of controllers on a stick-insect simulation

As a proof of principle the front-, middle-, and hind-leg controllers tested on the simulated robotic model were also tested on a simulated stick insect model. By only modifying "free" parameters (cp. Sect. 2.2.2), qualitatively comparable stepping behavior could be produced. Neither the structure of the controller nor those parameters prescribed by neuro-biological data were modified. Detailed data and parameters are given in Supplementary section S3. Major differences that could be observed were, despite the obvious differences due to scaling like locomotor speed, shorter step cycles, and differently shaped foot trajectories.

3.4 Support forces

3.4.1 Dorso-ventral forces

Are the single-leg controllers shown above suitable as control modules in hexapod controllers? To answer this question, their ability to support the body together with the mechanical system was investigated. Testing front-, middle-, and hind-legs with the controllers given above and neural parameter sets given in Supplementary sections S4.3, S4.4, and S4.5 showed that hind-legs and respective controllers could support body weight much more than middle-and front-legs, and that middle-legs would slightly outperform front-legs (see Fig. 15a G0). This order was similar to the one found for stick insects walking on flat terrain by Cruse (1976) (see Fig. 15b). To verify that this finding was not due to hand-tuned parameters, parameter optimization was performed: The goal was to reach maximum walking speed with maximum body support force (details are given in Sect. 2.4 "Parameter Optimization"):

1. First, a restricted parameter set, consisting of motor neuron bias values, all synapse weights with motor neurons as targets, and all premotor neuron bias values, was optimized. Maximum support forces by front- and middle-legs increased with progressing parameter optimization, but leveled off in the same order as the hand-tuned controller forces. Kinematics of optimized controllers (not shown) did not change much except that foot trajectories became more flat.
2. Second, almost all parameters (except internal parameters of the two-joint height control module) were made accessible to parameter optimization to check if extended parameter changes would allow front- and middle-leg controllers to develop similar support forces as the hind-leg controllers. As shown in Fig. 15 this is the case. Kinematics of optimized controllers (not shown) did change in such a way that not only the foot trajectories became more flat, but also the movement range of the FTi joint was decreased, and the mean tibia position became more vertical with respect to the ground.

3.4.2 Medio-lateral Forces

Figure 15 shows that controllers with initially hand-tuned parameters sequentially displayed forces in medial and in lateral directions, unlike in the single legs in in vivo hexapod walking that almost exclusively displayed medial-directed forces. Maximum forces were slightly larger in middle- and hind-legs but also front-legs showed non-negligible lateral forces, again different from the in vivo hexapod data. In both the parameter optimization cases (restricted and unrestricted, see above for details) lateral forces vanished with progressing optimization, becoming more similar to the in vivo example. The front-leg medio-lateral forces, though smaller in magnitude than in middle- and hind-legs, persisted.

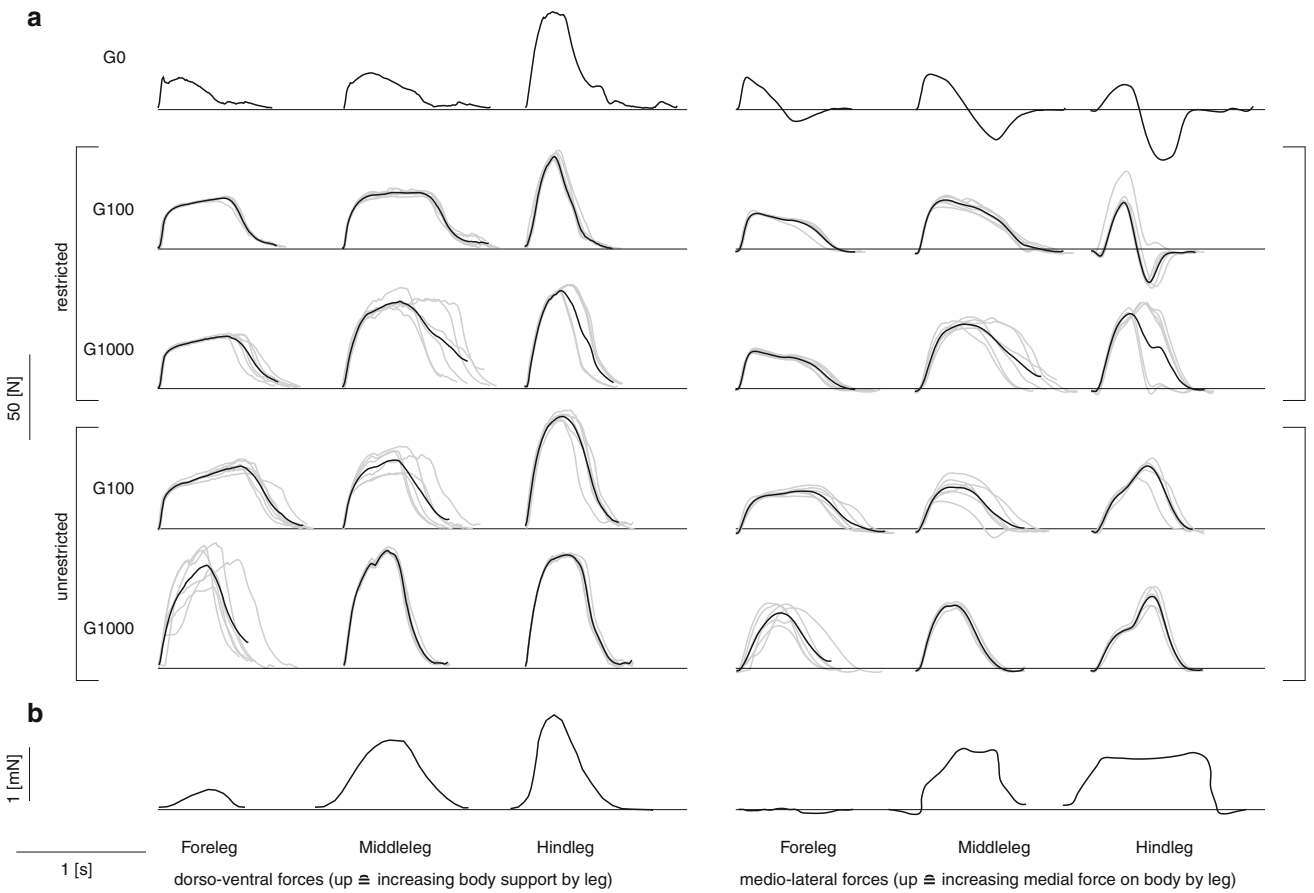

Fig. 15 Dorso-ventral and medio-lateral torso support forces (directions correspond to *y*- and *z*-axes in Fig. 6) by single legs: **a** in simulation (measured were forces between torso and rail suspension during forward walking) for hand tuned (G0) and parameter optimized controllers (G100 after 100 generations, G1000 after 1000 generations, restricted means optimization was only performed on a limited parameter set, cp. section 2.4.2) driving front-, middle-, and hind-legs. For each situation six independent parameter optimizations were run and for each best controller forces of five consecutive step cycles were averaged (*gray lines*). Force profiles of all six controllers were again averaged to give the mean forces which are shown as *black solid lines* (see text for details). **b** In in vivo stick insect hexapod walking on a plane (ground reaction forces of the feet, data taken from Fig. 7 in Cruse 1976). Note that time between force profiles of different legs has no meaning in single-leg experiments compared to the hexapod experiments by Cruse (1976)

4 Discussion

4.1 Deriving modular neural controllers

4.1.1 Feasibility of modular neural network implementation

Ekeberg et al. (2004) showed in simulation how simple modules coupled in the sensori-motor loop may constitute a clearly structured controller (cp. Fig. 1) producing robust behavior. Thus, using the modular approach to neural networks (Pasemann 1995; Pasemann et al. 2001; Manoonpong et al. 2008; Hülse and Pasemann 2006), it was a feasible task to translate the finite state controller model into an equivalent neural network controller consisting of simple neuro-modules (see Figs. 4, 5). Most of the network parameters were derived from parameters of the finite state controller by simple rules. Nevertheless, some details had to be addressed: (1) In the original paper timing control was done by the finite state controller, magnitude control (e.g., CTr height control) integrated into muscle activation functions. Here, both features are integrated into a single neuro-controller using corresponding neuro-modules, thus leading to a more transparent structure. (2) No absolute torques and joint velocities, corresponding to specific muscle activations, were given, therefore, muscle activations (here corresponding to premotor to motor synapse weights) had to be determined experimentally. (3) Multiple rules acting on a single joint could show contradictory outputs (and actually did so in behaviorally relevant situations, see Sect. 3), but the original publication does not state how these conflicts are resolved. Experiments showed

that prioritizing the rules as indicated in Sect. 2.1 and Fig. 1 was a successful strategy and the authors of Ekeberg et al. (2004) confirmed that they used the same strategy.

4.1.2 Benefits and limitations

In addition to the advantages mentioned in Sect.1 (e.g., easy deployment on hardware and usage as modules in artificial evolution) the neural implementation had some limitations: (1) Without proper documentation of the modular structure, the functionality of the modules and the meaning of parameters (e.g., thresholds represented by dimensionless bias values) was not as clear as in the finite state controller. Therefore, a detailed description of the modules, including a clearly structured neural network layout and conversion tables for important parameters, was indispensable. (2) As usually done in recurrent networks without distinct layers, the neural network was updated in the order activations → outputs with a frequency feasible for robot control. As a consequence significant time-delays could result. With the update frequency of 100 Hz that was used throughout all experiments the maximum time delay was 40 ms with four synapses between sensor and motor neuron (cp., e.g., pathway 7 → 12 in Fig. 4). To decrease this time-delay either the update rule had to be modified adding complexity to the system or the global update frequency had to be increased which was not desired on the robotic system Octavio. (3) Using single neurons as threshold approximators together with precision limits given by the hardware did not allow the same sharpness in transition as $if - else$ statements. Yet the neuro-threshold-modules employed in this context showed to have, in terms of behavior control, sufficiently sharp transitions and an increased benefit of noise robustness due to a hysteresis effect (see Supplementary Fig. S1).

4.2 Testing controllers on a robotic and a stick insect model

Successful tests of modular single-leg neuro-controllers with identical structure on a simulated model of the physical robot Octavio as well as on a simulated stick insect model demonstrated the controllers robust performance despite large differences in scaling and biomechanics:

4.2.1 Differences in mechanical plant and scaling

In comparison with stick insects (or simulated models thereof) basic morphological features of the simulated walking machine Octavio, like number of legs, number of main leg joints, joint axes and main sensory qualities, were similar. One exception was the ThC joint axis which only had one DOF in the robot and was parallel to the dorsal-ventral body axis. In the stick insect it has two DOF but one main functional DOF and this axis has an offset to the dorsal-ventral body axis (Cruse and Bartling 1995). It is argued that the medio-ventral to lateral-dorsal joint axis simplifies stance control: in the stick insect, by only performing a retraction movement, the leg is automatically loaded and unloaded during stance phase, not requiring the control of other joints.

Despite differences in scale (cp. Supplementary Table. S1) geometric similarity and pre-conditions for dynamic similarity (Alexander 1989) were roughly given (cp. Supplementary section S2). Additionally increased stress, which is thought to cause larger animals to hold their legs straighter during walking (Biewener 2005), was not a problem in the simulation of the scaled up robotic model used here. So this would have to be tested in the physical robot, taking into account differences between muscle-tendon and technical motor-gear-spring systems. Comparatively slow walking of stick insects, resulting in duty factors being much larger than in running animals, reduced the stress problem to some extent. Furthermore, limb size influence on unloaded limb motor control strategy as discussed in Hooper et al. (2009) did not qualitatively change the behavior of the scaled up model. This was attributed to the direction of the controller transfer: in small animals like stick insects persistent swing motor neuron activations are necessary to complete swing phase. But the same control strategy also worked for the robot Octavio where inertia was large when compared to joint friction. The alternative control strategy of larger animals requires motor neuron activity only during acceleration and deceleration phases due to their ballistic limb movements. This would not be applicable to small animals where antagonist muscle passive forces and cuticular passive forces are larger than gravitational forces.

4.2.2 Motor versus muscle systems

Using virtual antagonists to drive one single motor-gear combination per joint in the robot (see Sect. 2.3 and Fig. 7 for details) seemed overly complicated but had several advantages: it increased comparability with biological controllers, it was better prepared for migration to a machine with real antagonists and some control concepts were realized in a simpler way when using the antagonist motor interface. This was, e.g., demonstrated for velocity control in the middle-leg (see Sect. 3.1.3). As a result of only having virtual antagonists real stiffness control by antagonist co-activation was not possible and muscle properties like force-length characteristics present in the stick insect (Guschlbauer et al. 2007) were missing in the real robot. Therefore, a different walking behavior was expected when using the controller transferred directly from biology. For all controllers transferred, except the restricted middle-leg one, modifications were necessary in the ThC joint control (and for the hind-leg also in the FTi joint control) to achieve robust walking behavior, adding

intra-joint position feedback leading to a stabilization of the joints working range. This may be thought of as a possible replacement for intra-muscular joint position feedback (or in other words position dependent actuation limiting feedback) due to the force-length characteristics. Ekeberg et al. (2004) used a simple linear muscle model and did not have to add this kind of intra-joint feedback in the ThC joint or in the FTI joint for the hind-leg controller. As in the hind-leg FTi joint the environment could also—at least to some extend—contribute to joint working range stabilization by imposing constraints on joint movement. This could have been due to, e.g., ground contact or gravitation. Rutter et al. (2007) compared the performance of controllers with a piecewise constant muscle model, a linear muscle model, and without a muscle model in the FTi joint. They found a more reliable ground contact detection when using any of the two muscle models. They attributed this to a reduced tibia extension at swing–stance transition improving performance of restricted and forward walking. In contrast, the swing–stance transitions were unproblematic in the model presented here. Probably this was due to using a ground contact sensor instead of a motor current ("load") sensor. An exception was the hind-leg controller where no intra-joint feedback in the FTi joint control module existed and this led to a fragile walking behavior (cp. Sect. 3.2). Adding FTi intra-joint feedback stabilized the system. Lewinger et al. (2006) also found a drift of the ThC movement toward extreme joint positions without muscle models and suggested that the underlying plant must exhibit saturation to show robust behavior. A forthcoming paper will specifically address the question of how requirements change for neural controllers due to the presence or absence of muscles or muscle models.

4.2.3 Performance of controllers

4.2.3.1 Kinematics As for the restricted middle-leg (cp. Section 3.1.1), kinematics of forward stepping was found to be similar to that in the stick insect, especially considering the differences between front-, middle-, and hind-legs (cp., e.g., Fig. 3 in Cruse and Bartling 1995 with Fig. 8 in this article). With one exception differences to observations in biology could be, as in the restricted preparation, explained by differences in parameter tuning and experimental setups: robust biphasic FTi movements during stance (Cruse and Bartling 1995) could only be achieved by structural changes in the neural controller (cp. Sect. 3.1.2). A ThC influence on flexion-extension transition resulted in robust walking with biphasic FTi movements during stance but has not been found in the stick insect nervous system. As an alternative a two-phase positive/negative FTi intra-joint velocity feedback termed the "active reaction" (Bässler 1988) is observed in stick insects and would lead to a stabilized flexion-extension transition during stance. Additionally muscle properties might play a stabilizing role.

4.2.3.2 Cycle periods Regarding minimum step cycle periods the robotic model came much closer to real stick insects when compared with Ekeberg et al. (2004). This was despite the scaling issues discussed above. Depending on parameters step cycle periods of 700 ms to several seconds resulted (see Figs. 10 and 11) compared to 600 ms to 2.5 s for the stick insect (Fischer et al. 2001). In contrast, Ekeberg et al. (2004) found cycle periods between 6 and 10 s. The much lower step frequencies in Ekeberg et al. (2004) were attributed to a slow swing movement caused by the linear muscle model. Unfortunately, no exact simulation parameters were given to allow for a better comparison. The shorter cycle periods in the stick insect model presented here (400 ms to several seconds, see Supplementary Figs. S6 and S7) were, in addition to parameter tuning, due to the lack of force attenuation with length and velocity changes as caused by muscles in the real stick insect. Minimal swing durations were still longer in the robot (350–600 ms) and stick insect (170–340 ms) simulations presented here than in the real stick insect ($\approx$ 100 ms, Wendler 1964; Graham 1985). In the robotic model, this was partly attributed to the slower actuators and in both models it was attributed to the swing control: muscle properties limiting FTi extension were lacking and therefore led to prolonged swing phases (cp. discussion above).

4.2.3.3 Magnitude control Differing from biological data (Cruse et al. 1993; Hess and Büschges 1997; Bucher et al. 2003), the height control module was not only active during stance but also during swing phase. Since it did not have exclusive access to the CTr motor neurons reasonable walking behavior was generated nevertheless, including kinematics similar to stick insect data (see above). Additionally, a gating mechanism may be introduced, disabling the height control module during swing or dynamically changing the height controls reference input via the CTr premotor neuron. Positive and negative velocity control during stance in the FTi joint (Bässler 1993; Bartling and Schmitz 2000) has not been taken into account, because it was not necessary for generating stable walking behavior and made the controller and resulting behavior more complicated to explain. In principle, two additional modules are required to add the velocity feedback: (1) an additional comparator module with FTi velocity as input and its output projecting to FTi motor neurons, and (2) an additional threshold element with FTi velocity as input and the comparator as target. The comparator then has to be gated by the FTi premotor neuron, only activating it during flexion (stance) phase.

4.2.3.4 Changing behavior by changing parameters As an example of behavior control by neural parameters velocity

control in the middle-leg was investigated in greater detail. Two different mechanisms influencing walking speed were found (cp. Sect. 3.1.3): the increase in velocity due to a decrease in stance phase duration with nearly constant swing duration and support length was also found in stick insects (Wendler 1964; Graham 1972; Graham and Cruse 1981; Gabriel and Büschges 2007). This is in contrast to the support length increase found for higher velocities in this study. In cats, the same mechanism was found (Goslow et al. 1973; Halbertsma 1983), but contrary to the stick insect absolute stance duration could become lower than absolute swing duration. In addition, support length changes contributing to velocity changes were found (Halbertsma 1983). As an underlying mechanism gain modulated sensory pathways and not purely central tonic influences are suggested in stick insects (Gabriel and Büschges 2007) as well as in cats (Yakovenko et al. 2005). Functionally, this mechanism agrees with the one presented here because stance phase motor neurons were completely deactivated during swing phase due to the bistable premotor elements. Therefore, the bias parameters of the stance motor neurons effectively modulated the gain of the sensory influences during stance. With a slightly more complicated structure a parallel gain modulated pathway from sensors to motor neurons could be easily implemented.

The current model failed to control slow velocities below ≈ 0.25 m/s in a robust way because small differences in joint torque would decide between slow movements or no movements. Under noisy conditions or changing environments some kind of an extra velocity feedback mechanism, e.g., a mechanism similar to the active reaction found in stick insects (Bässler 1993) and/or muscular properties (Guschlbauer et al. 2007), would be required.

For animals or walking machines velocity control cannot be restricted to single-legs only, but rather multiple legs have to be coordinated. In stick insects neural coupling of leg velocities have only been found under some circumstances, e.g., in accelerating animals, and mechanical coupling between legs together with muscular properties are discussed as main factors (Gruhn et al. 2009). In Fig. 13c (simulated up- and downhill walking), it is shown that the current model could—without any neural parameter changes or central neural influences—adapt its velocity to changing environmental conditions, mainly due to stance phase duration changes. This is beneficial for an efficient mechanical coupling of multiple legs and leg controllers as modules of a hexapod controller.

4.2.3.5 Controller robustness In Sect. 3.1.4, the middle-leg controllers were demonstrated to be robust under multiple experimental perturbing conditions (von Twickel and Pasemann 2007; Revzen et al. 2009) without matching the extreme flexibility exhibited by stick insects (see, e.g., Cruse et al. 2004; Blaesing and Cruse 2004). The latter would only have been possible if hypothetical extensions were made to the controller structure, e.g., to deal with specific reflexes, as is the case with functional modeling approaches (see below for a detailed discussion). Hereafter, differences in behavior between the stick insect and robotic model, driven by the presented controllers, are discussed for the various perturbing conditions. On the single-leg level, one has to differentiate between disturbances occurring during swing and stance phases. In swing phase, the leg is mechanically uncoupled from other legs. In stance phase, the leg is mechanically coupled to the ground and all legs that are in stance phase at the same time (Bartling and Schmitz 2000).

In a first simulation (see, Fig. 13a), ground height was randomly varied relative to body suspension height without disrupting walking behavior. On the one hand, this was consistent with findings by Lewinger et al. (2006) who demonstrated their implementation of the Ekeberg controller to be robust against body height changes and against initial conditions. On the other hand, the observed behavior was only partly consistent with behavioral data from the stick insect as shown for the swing phase dependence on take off position in Fig. 14. Simulation results were compared with data from Schumm and Cruse (2006), where swing trajectories were examined under varying PEP start positions: small variations in anterior-posterior AEP positions and a negative correlation of dorsal-ventral swing amplitude and PEP height were consistent although swing height dependence on anterior-posterior and dorsal-ventral PEP positions could not be differentiated. A predominant swing height dependence on PEP height and not on anterior posterior PEP position made sense from the mechanistic point of view: Levation velocity (cp. Fig. 14d) mainly determined swing height and was dependent on the CTr height control module. The height control module produced larger levation activations for larger dorsal-ventral torso-tarsus distances but independent of the anterior posterior tarsus position. Nevertheless, a larger influence of FTi(γ)-angle at PEP on swing height for varying anterior-posterior PEPs has to be disproved experimentally. Its potential influence became obvious when investigating the "outliers" regarding swing height for extreme low and high PEPs in Figs. 13a and 14: Depending on the environmental conditions the FTi(γ)-angle at the beginning of swing could vary quite substantially leading to a variation in the duration of the initial swing phase (PEP–SEP). Two basic strategies could be applied to stabilize swing movements over a larger PEP height range and to achieve a closer match with biological data: first, FTi-movement could be stabilized via, e.g., a velocity and/or position servo mechanism or a muscle model to result in less varying FTi-angles at the beginning of stance. Second, swing height could be controlled independently of FTi-angle at PEP via controlling, e.g., the extension velocity during swing.

In a second simulation (see Fig. 13b), the regular walking pattern was not interrupted and swing trajectories were almost unaffected by lateral force applications ("kicks"). Exceptions were compliant lateral torso and tarsus movements during force application. Since no control module dealing explicitly with disturbances during stance (except the height controller) was contained in the leg controller, this result showed the implicit robustness of the bio-mechanical system together with the sensori-motor control, which does not explicitly control trajectories. More sophisticated reactions resisting or assisting perturbations and maintaining stability despite larger perturbation amplitudes would require extensions to the current controller, like, e.g., negative and positive velocity feedback mechanisms found in stick insects (Bartling and Schmitz 2000) and/or muscle like actuator properties. The observed lateral compliance seems favorable for coupling multiple legs in contrast to a very stiff-controlled trajectory.

As shown in Fig. 13c, robust walking behavior was maintained and locomotion velocity was adapted to different loading conditions, simulating "uphill" and "downhill" walking. This was mainly due to stance duration variations and to a minor extend due to a slightly increased support length (together with a posteriorly shifted PEP) during "downhill" walking. The decrease in velocity with increasing resistance forces was also found in single-leg treadmill experiments in stick insects with different levels of belt friction (≈15–75% of body weight) by Gabriel et al. (2003): Together with an increase in slow and fast motor neuron firing rates forces applied to the treadmill increased while peak velocities decreased with increasing levels of belt friction. In Cruse (1976), stick insects climbing up a vertical path (corresponding to 100% force of body weight against walking direction) AEP and PEP shifted rostrally, in addition to a general increase in stride amplitude. Both were discussed in the context of mechanical and muscular advantages in terms of upwards force production. Rostrally shifted PEPs during uphill walking are consistent with the results presented here as opposed to the AEPs and the support length increase which was observed in the simulation for "downhill" walking. In Foth and Graham (1983), static- and velocity-dependent loads were applied to the two sides of a split treadwheel separately with load amplitudes between 12.5 and 100% of body weight. In addition to the findings of Cruse (1976) it was found that forces up to ≈40% of body weight per side (corresponding to 20% in wave gait and 40% in tripod gait) were compensated by raises in muscle forces. Above ≈40% force of body weight, protraction duration was reduced to a minimum and became independent of step period, and retraction duration increased with increases in load. Dean (1991) applied different levels of static force (0.5–4 time body weight) assisting or resisting forward walking. In addition to the above-mentioned studies he found swing duration increases for larger resisting loads. Furthermore, he put forth the hypothesis that the retractor relaxation after strong stances is slower and therefore leads to slower and longer swing movements. When comparing the presented experiments with stick insect data it is important to consider that most experiments have been performed with multiple legs and at non-maximal locomotion speed. Here walking speed was close to maximum and only a single-leg was active. For a more detailed comparison with biological data, our model should first be extended by muscular properties and/or load and velocity feedback control mechanisms, and then load adaptations under different velocities should be tested.

Robust stepping up to noise levels of ≈40% on all motor neuron outputs or up to ≈15% on all sensor-neuron inputs (cp. Fig. 13d, e) is qualitatively comparable to the experiments by Ekeberg et al. (2004): they showed that the original controller is robust (in the sense of qualitatively preserved behavior) against single random variations of threshold angles in a range of ±5° and of muscle activation values of ±50%. Kindermann (2002) obtained similar sensor noise tolerances (7–17%, depending on conditions) for a simulated hexapod but did not test motor noise tolerance. These noise tolerance tests can be seen as a rough sensitivity analysis. Motor- and bio-mechanical systems show to have a higher tolerance against noise than the neural system deriving the joint activation states from sensor inputs. We attribute this to the low pass filter characteristics of the mechanical system being much stronger than those of the joint state switching elements of the neural system. These are, in the neural implementation, realized as hysteresis elements. Including realistic muscle models, which have activation functions with strong low pass filter characteristics as in the stick insect (Hooper et al. 2007), should even increase the noise tolerance of the bio-mechanical system.

4.2.3.6 Body support forces For both vertical and medio-lateral body support forces (cp. Sect. 3.4) it was found that force profiles could be altered by tuning "free" neural parameters, i.e., parameters not prescribed by the neural rules. By additionally tuning, e.g., threshold parameters force profiles could be altered even more, also changing kinematics. This demonstrated the controllers flexibility to adapt to different body support requirements.

For vertical forces it was shown that force profiles of optimized controllers, with kinematics similar to the one found in biology, resulted in similar force profiles (Cruse 1976; Bartling and Schmitz 2000). Body support forces could be much higher for hind-legs than for middle- and front-legs. This is consistent with the requirement in the stick insect that hind-legs have to carry most of the body weight because their center of mass is located between them (Cruse 1976). In Bartling and Schmitz (2000), vertical front-leg forces were

found to be so weak that they could not be reliably used as a trigger signal. In contrast to the results shown here and in Cruse (1976) the same study found vertical forces of the middle-leg to be slightly larger than in hind-legs. In contrast to stick insects, front-legs of cockroaches have comparable vertical ground-reaction forces as middle- and hind-legs (Full et al. 1991). This in turn means that walking machines and animals with a different mass distribution might require different force profiles and possibly also different leg kinematics. Additionally, the differences in joint axes setup when compared to the stick insect, especially slanted ThC joint axes in the ThC joint of the stick insect (Cruse and Bartling 1995), might have a significant influence on the ground reaction forces during stance.

A lack of lateral-directed body forces in parameter optimized controllers is again comparable to biological data, with the exception of the front-leg where lateral forces are negligible (Cruse 1976; Bartling and Schmitz 2000). In animals and robots it has been shown that medial-directed forces from legs to the body are important to laterally stabilize posture and walking behavior (Dickinson et al. 2000; Komsuoglu et al. 2009).

In general different force profiles by the three leg types reflect their specialization, e.g., for pushing, pulling, and generating brake forces (see, e.g., Graham 1983; Full et al. 1991). Further issues like force coordination between legs have to be investigated in the context of hexapod walking, e.g., the force coordination problem between legs (Lévy and Cruse 2008).

4.2.3.7 Comparison with existing controllers First of all it has to be noted that the presented controllers share many structural and functional similarities with other walking controller models of stick insects, cats, and humans. Similarities include the modular organization and the strong role of sensory feedback in timing (e.g., swing–stance and stance–swing transitions) and in magnitude control (e.g., negative feedback control of body height). These aspects have been discussed at length before (see, e.g., Dürr et al. 2004; Ekeberg et al. 2004; Büschges 2005; Pearson et al. 2006). In the following, we will, therefore, focus our discussion on a different aspect. Two basic approaches appear to be used to derive walking controllers from biological data (Cruse et al. 2007): the "morphological" approach, as taken in Ekeberg et al. (2004) and in the study presented here, incrementally builds up a controller from available neuro-biological data and information about the bio-mechanical system. Subsequently, it compares its behavior with that of the natural counterpart. In contrast, the "functional" approach builds up controllers with the primary goal to match behavioral data, not focusing on direct correlations with the neural substrate of the stick insect.

The latter approach has been pursued by Cruse and coworkers over the last two decades resulting in multiple iterations of the WALKNET controller (see, e.g., Dürr 2001; Schumm and Cruse 2006; Kindermann 2002; Cruse et al. 2004; Cruse et al. 2007). WALKNET constitutes a distributed controller which heavily depends on sensory feedback, whereby the (partly positive) feedback is mainly of proprioceptive nature. WALKNET describes, to an extent unmatched by other approaches, the behavioral repertoire of the six-legged stick insect. In addition to its advantages, three main problems of the current WALKNET implementation were identified: (1) As a principle problem of the functional approach the correlation of model controller structure with biological controller structure is difficult. From a theoretical point of view (Negrello et al. 2008) one and the same functionality may be produced by an arbitrary number of control structures and therefore WALKNET is only one of many possible controller structures able to produce the stick insect behavior. (2) WALKNET was developed in a kinematic simulation and therefore does not incorporate load information (but see Schilling et al. (2007) for such an extension) or detailed muscle properties. (3) In contrast to its mostly distributed structure it uses a leg global swing–stance selector net. By now no neuro-biological evidence has been presented that different neural controllers for stance and swing exist. All neuronal elements analyzed so far affect the motor output during both stance and swing phase (Büschges et al. 1994; Wolf and Büschges 1995; von Uckermann and Büschges 2009).

The "morphological" approach taken here addresses these three problems whereby the possibility of controller structure correlation is self-evident. Load information and muscle properties have already been implemented in the dynamic simulation presented here (see also Sect. 3.4) and their influence on controller performance will be subject of a forthcoming publication. Concerning the "swing–stance selector net" a completely decentralized solution was employed: Only one structure existed for the control of both swing and stance and each joint locally decided about its movement phase. Each joint possessed a bistable premotor element with hysteresis properties that held the desired movement direction, e.g., levation or depression for the CTr joint. The desired direction could be overridden by parallel inputs to the motor neurons as was, e.g., the case for the height controller in the CTr joint. Although this solution appears to be more elegant, it has yet to be demonstrated how more complex behaviors like different disturbance reflexes may work without a central selector network. We argue that the decision between swing and stance is an emergent property of the neuro-mechanical system, and locally this decision is deduced from multiple sensor- and neural-inputs.

When compared to the WALKNET controller the "morphological" controller presented here had some shortcomings:

first of all discrepancies existed between the behavior produced by the single-leg controller, on the one hand, and that produced by the stick insect, on the other hand (see Sects. 4, 3 above). Then the neural data available is not yet sufficient to build up a hexapod walking controller or controllers producing similarly complex behaviors as WALKNET. First steps have been taken on the neuro-biological side (Borgmann et al. 2009) and on the modeling side (Daun-Gruhn 2010) toward a hexapod controller based on neuro-biological data. Further experiments will have to show if the current single-leg controller structure is sufficient to act as a leg control module of a hexapod controller or if non-trivial extensions are necessary. Furthermore, the approach taken here employed different controller structures for front- and middle-legs, on the one hand, and hind-legs, on the other hand. In contrast, WALKNET is able to produce the different behaviors by the same controller structure but using different parameter sets. The latter approach simplifies a modular implementation on robots but its neuro-biological relevance has yet to be shown. Theoretically, even controllers with identical structures and parameters could achieve a similar functional diversity by just differing in biomechanics, sensory inputs or coupling influences.

In a complementary approach to the two basic biological modeling approaches the artificial life approach to evolutionary robotics is employed to derive minimal controllers, producing walking behaviors similar to that of the stick insects (see, e.g., von Twickel and Pasemann 2007; Linder 2005). Comparing the controller structure presented here with the ones found in von Twickel and Pasemann (2007), containing, e.g., only four synapses, the question arises of why a larger controller structure is needed at all. To one part this is due to the latter study working with single neuron servo interfaces, already including intra-joint sensory feedback and not requiring premotor neurons for antagonistic activations. To another part, the advantage might be increased redundancy and therefore increased robustness against failures. Otherwise the advantage of a more complicated structure is not obvious and one will have to compare these different controller types in detail on single-legs and as modules for hexapod controllers.

5 Conclusion and outlook

A step-by-step method for deriving a neural network model from neuro-biological data via an intermediate finite state model was presented. Properties of single front-, middle-, and hind-leg controllers were demonstrated including their robustness under multiple experimental perturbations, their flexibility in terms of body support forces, and feasible behavior modifications by parameter tuning. The modular structure of the controller allows for easy extendability, and its neural network implementation will simplify their transfer to walking machines. Taken together, the robustness and flexibility of the described controllers make them promising bootstrap modules for future evolutionary coupling experiments. Therefore, this study is seen as a step toward the integration of behavioral and neural-based approaches to locomotion control, and—on the other hand—as a first step toward the derivation of robust hexapod controllers for walking machines.

Acknowledgments This study was supported by DFG grants (Pa 480/6-1 and Bu 857/9-1). We would like to thank Holk Cruse and the anonymous reviewers for valuable comments, and Marcus Blümel and Christian Rempis for helpful discussions.

References

Alexander RM (1989) Optimization and gaits in the locomotion of vertebrates. Physiol Rev 69:1199–1227

Azevedo C, Espiau B, Amblard B, Assaiante C (2007) Bipedal locomotion: toward unified concepts in robotics and neuroscience. Biol Cybern 96:209–228

Bartling C, Schmitz J (2000) Reaction to disturbances of a walking leg during stance. J Exp Biol 203:1211–1223

Bässler U (1983) Neural basis of elementary behavior in stick insects. Springer, Berlin

Bässler U (1988) Functional principles of pattern generation for walking movements of stick insect forelegs: the role of the femoral chordotonal organ afferences. J Exp Biol 136:125–147

Bässler U (1993) The femur-tibia control system of stick insects a model system for the study of the neural basis of joint control. Brain Res Rev 18(2):207–226

Bässler U, Büschges A (1998) Pattern generation for stick insect walking movements—multisensory control of a locomotor program. Brain Res Rev 27:65–88

Beer RD (2006) Beyond control: the dynamics of brain-body-environment interaction in motor systems. In: Sternard DProgress in motor control V: a multidisciplinary perspective. Springer, Berlin pp 7–24

Beer RD, Quinn RD, Chiel HJ, Ritzmann RE (1997) Biologically inspired approaches to robotics—what can we learn from insects. Commun ACM 40(3):31–38

Bekey GA (2005) Autonomous robots—from biological inspiration to implementation and control. MIT Press, Cambridge

Biewener AA (2005) Biomechanical consequences of scaling. J Exp Biol 208:1665–1676

Blaesing B, Cruse H (2004) Stick insect locomotion in a complex environment: climbing over large gaps. J Exp Biol 207:1273–1286

Borgmann A, Scharstein H, Büschges A (2007) Intersegmental coordination: influence of a single walking leg on the neighboring segments in the stick insect walking system. J Neurophysiol 98:1685–1696

Borgmann A, Hooper SL, Büschges A (2009) Sensory feedback induced by front-leg stepping entrains the activity of central pattern generators in caudal segments of the stick insect walking system. J Neurosci 29(9):2972–2983

Brunn DE, Dean J (1994) Intersegmental and local interneurons in the metathorax of the stick insect carausius morosus that monitor middle leg position. J Neurophysiol 72(3):1208–1219

Bucher D, Akay T, DiCaprio RA, Büschges A (2003) Interjoint coordination in the stick insect leg-control system: the role of positional signaling. J Neurophysiol 89:1245–1255

Büschges A (2005) Sensory control and organization of neural networks mediating coordination of multisegmental organs for locomotion. J Neurophysiol 93:1127–1135

Büschges A, Kittmann R, Schmitz J (1994) Identified nonspiking interneurons in leg reflexes and during walking in the stick insect. J Comp Physiol A 174:685–700

Büschges A, Akay T, Gabriel JP, Schmidt J (2008) Organizing network action for locomotion: insights from studying insect walking. Brain Res Rev 57:162–171

Calvitti A, Beer RD (2000) Analysis of a distributed model of leg coordination i. Individual coordination mechanisms. Biol Cybern 82:197–206

Chiel HJ, Ting LH, Ekeberg O, Hartmann MJZ (2009) The brain in its body: Motor control and sensing in a biomechanical context. J Neurosci 29(41):12807–12814

Cruse H (1976) The function of the legs in the free walking stick insect, carausius morosus. J Comp Physiol A 112:235–262

Cruse H (1980) A quantitative model of walking incorporating central and peripheral influences i. The control of the individual leg. Biol Cybern 37:131–136

Cruse H (1990) What mechanisms coordinate leg movement in walking arthropods. Trends Neurosci 13:15–21

Cruse H, Bartling C (1995) Movement of joint angles in the legs of a walking insect, carausius morosus. J Insect Physiol 41(9):761–771

Cruse H, Schmitz J, Braun U, Schweins A (1993) Control of body height in a stick insect walking on a treadwheel. J Exp Biol 181(1):141–155

Cruse H, Kühn S, Park S, Schmitz J (2004) Adaptive control for insect leg position: controller properties depend on substrate compliance. J Comp Physiol A 190(12):983–991

Cruse H, Dürr V, Schmitz J (2007) Insect walking is based on a decentralized architecture revealing a simple and robust controller. Philos Trans R Soc A 365(1850):221–250

Daun-Gruhn S (2010) A mathematical modeling study of inter-segmental coordination during stick insect walking. J Comput Neurosci, pp 1–24. http://dx.doi.org/10.1007/s10827-010-0254-3, online first

Dean J (1991) Effect of load on leg movement and step coordination of the stick insect carausius morosus. J Exp Biol 159:449–471

Dickinson MH, Farley CT, Full RJ, Koehl MAR, Kram R, Lehmann S (2000) How animals move: an integrative view. Science 288:100–106

Dürr V (2001) Stereotypic leg searching movements in the stick insect: kinematic analysis, behavioural context and simulation. J Exp Biol 204:1589–1604

Dürr V (2005) Context-dependent changes in strength and efficacy of leg coordination mechanisms. J Exp Biol 208:2253–2267

Dürr V, Schmitz J, Cruse H (2004) Behaviour-based modelling of hexapod locomotion: linking biology and technical application. Arthropod Struct Dev 33:237–250

Ekeberg O, Blümel M, Büschges A (2004) Dynamic simulation of insect walking. Arthropod Struct Dev 33:287–300

Fischer H, Schmidt J, Haas R, Büschges A (2001) Pattern generation for walking and searching movements of a stick insect leg. i. Coordination of motor activity. J Neurophysiol 85:341–353

Foth E, Graham D (1983) Influence of loading parallel to the body axis on the walking coordination of an insect—I. Ipsilateral effects. Biol Cybern 47(1):17–23

Frigon A, Rossignol S (2006) Experiments and models of sensorimotor interactions during locomotion. Biol Cybern 95(6):607–627

Full RJ, Blickhan R, Ting LH (1991) Leg design in hexapedal runners. J Exp Biol 158:369–390

Gabriel JP, Büschges A (2007) Control of stepping velocity in a single insect leg during walking. Philos Trans R Soc A 365: 251–271

Gabriel JP, Scharstein H, Schmidt J, Büschges A (2003) Control of flexor motoneuron activity during single leg walking of the stick insect on an electronically controlled treadwheel. J Neurobiol 56:237–251

Ghazi-Zahedi KM (2008) Self-regulating neurons. A model for synaptic plasticity in artificial recurrent neural networks. PhD thesis, University of Osnabrück

Goslow GE, Reinking RM, Stuart DG (1973) The cat step cycle: hind limb joint angles and muscle lengths during unrestrained locomotion. J Morphol 141(1):1–41

Graham D (1972) A behavioural analysis of the temporal organization of walking movements in the 1st instar and adult stick insect *Carausius morosus*. J Comp Physiol 81:23–52

Graham D (1983) Insects are both impeded and propelled by their legs during walking. J Exp Biol 104:129–137

Graham D (1985) Pattern and control of walking in insects. Adv Insect Physiol 18:31–140

Graham D, Cruse H (1981) Coordinated walking of stick insects on a mercury surface. J Exp Biol 92:229–241

Grillner S (2006) Biological pattern generation: the cellular and computational logic of networks in motion. Neuron 52(5):751–766

Gruhn M, von Uckermann G, Westmark S, Wosnitza A, Büschges A, Borgmann A (2009) Control of stepping velocity in the stick insect carausius morosus. J Neurophysiol 102:1180–1192

Guschlbauer C, Scharstein H, Büschges A (2007) The extensor tibiae muscle of the stick insect: biomechanical properties of an insect walking muscle. J Exp Biol 210:1092–1108

Halbertsma J (1983) The stride cycle of the cat: the modelling of locomotion by computerized analysis of automatic recordings. Acta Physiol Scand Suppl 521:1–75

Hatsopoulos NG (1996) Coupling the neural and physical dynamics in rhythmic movements. Neural Comput 8:567–581

Hess D, Büschges A (1997) Sensorimotor pathways involved in interjoint reflex action of an insect leg. J Neurobiol 33(7):891–913

Hooper SL, Guschlbauer C, von Uckermann G, Büschges A (2007) Slow temporal filtering may largely explain the transformation of stick insect (carausius morosus) extensor motor neuron activity into muscle movement. J Neurophysiol 98:1718–1732

Hooper SL, Guschlbauer C, Blümel M, Rosenbaum P, Gruhn M, Akay T, Büschges A (2009) Neural control of unloaded leg posture and of leg swing in stick insect cockroach, and mouse differs from that in larger animals. J Neurosci 29(13):4109–4119

Hülse M, Pasemann F (2006) Modular design of irreducible systems. In: Nolfi S, et al (eds) From animals to Animats 9 (SAB 2006), LNAI, vol 4095. Springer, Berlin. pp 534–545

Hülse M, Wischmann S, Pasemann F (2004) Structure and function of evolved neuro-controllers for autonomous robots. Connect Sci 16(4):249–266

Hülse M, Wischmann S, von Twickel A, Manoonpong P, Pasemann F (2007) Dynamical systems in the sensorimotor loop—on the interrelation between internal and external mechanisms of evolved robot behavior. In: Lungarella M, et al (eds) 50 years of artificial intelligence, LNAI, vol 4850. Springer, Berlin, pp 186–195

Ijspeert A, Crespi A, Ryczko D, Cabelguen JM (2007) From swimming to walking with a salamander robot driven by a spinal cord model. Science 315(5817):1416–1420

Ijspeert AJ (2008) Central pattern generators for locomotion control in animals and robots: a review. Neural Netw 21(4):642–653

Kindermann T (2002) Behavior and adaptability of a six-legged walking system with highly distributed control. Adapt Behav 9(1):16–41

Komsuoglu H, Sohn K, Full RJ, Koditschek DE (2009) A physical model for dynamical arthropod running on level ground. In: Khatib O, et al (eds) Experimental robotics—the eleventh international symposium, Springer, pp 303–317

Lévy J, Cruse H (2008) Controlling a system with redundant degrees of freedom: II. Solution of the force distribution problem without a body model. J Comp Physiol A 194(8):735–750

Lewinger WA, Rutter BL, Blümel M, Büschges A, Quinn RD (2006) Sensory coupled action switching modules (SCASM) generate robust, adaptive stepping in legged robots. In: Proceedings of the 9th international conference on climbing and walking robots (CLAWAR 2006), Brussels

Linder CR (2005) Embodiment in two dimensions. In: Proceedings of the 7th international conference on climbing and walking robots, 2004

Ludwar BC, Göritz ML, Schmidt J (2005) Intersegmental coordination of walking movements in stick insects. J Neurophysiol 93:1255–1265

Manoonpong P, Pasemann F, Wörgötter F (2008) Sensor-driven neural control for omnidirectional locomotion and versatile reactive behaviors of walking machines. Robot Auton Syst 56(3):265–288

Maufroy C, Kimura H, Takase K (2008) Towards a general neural controller for quadrupedal locomotion. Neural Netw 21:667–681

Negrello M, Hülse M, Pasemann F (2008) Adaptive neurodynamics. In: Yang A, Shan YApplications of complex adaptive systems. Idea Group, Hershey pp 85–111

Nolfi S, Floreano D (2000) Evolutionary robotics: the biology, intelligence, and technology of self-organizing machines. MIT Press, Cambridge

Orlovsky G, Deliagina T, Grillner S (1999) Neuronal control of locomotion. Oxford University Press, Oxford

Pasemann F (1995) Characterization of periodic attractors in neural ring networks. Neural Netw 8:421–429

Pasemann F, Steinmetz U, Hülse M, Lara B (2001) Robot control and the evolution of modular neurodynamics. Theory Biosci 120:311–326

Pearson K, Iles J (1973) Nervous mechanisms underlying intersegmental co-ordination of leg movements during walking in the cockroach. J Exp Biol 58:725–744

Pearson K, Ekeberg O, Büschges A (2006) Assessing sensory function in locomotor systems using neuro-mechanical simulations. Trends Neurosci 29(11):625–631

Pfeifer R, Bongard J (2006) How the body shapes the way we think—a new view of intelligence. MIT Press, Cambridge

Revzen S, Koditschek DE, Full RJ (2009) Towards testable neuromechanical control architectures for running. In: Sternad D (ed) Progress in motor control—a multidisciplinary perspective, Advances In Experimental Medicine And Biology, vol 629. Springer, Berlin, pp 25–56

Ritzmann RE, Büschges A (2007) Insect walking: from reduced preparations to natural terrain. In: North G, Greenspan RJ (eds) Invertebrate neurobiology. Cold Spring Harbor Laboratory, Cold Spring Harbor pp 229–250

Rutter BL, Lewinger WA, Blümel M, Büschges A, Quinn RD (2007) Simple muscle models regularize motion in a robotic leg with neurally-based step generation. In: 2007 IEEE international conference on robotics and automation, Roma, pp 630–635

Schilling M, Cruse H, Arena P (2007) Hexapod walking: an expansion to walknet dealing with leg amputations and force oscillations. Biol Cybern 96(3):323–340

Schumm M, Cruse H (2006) Control of swing movement: influences of differently shaped substrate. J Comp Physiol A 192(10):1147–1164

Smith R (2009) Open dynamics engine. http://www.ode.org, last visited: 18/11/2009

von Twickel A, Pasemann F (2007) Reflex-oscillations in evolved single leg neurocontrollers for walking machines. Nat Comput 6(3):311–337

von Uckermann G, Büschges A (2009) Premotor interneurons in the local control of stepping motor output for the stick insect single middle leg. J Neurophysiol 102:1956–1975

Webb B (2009) Animals versus animats: or why not model the real iguana. Adapt Behav 17(4):269–286

Wendler G (1964) Laufen und stehen der stabheuschrecke carausius morosus: sinnesborstenfelder in den beingelenken als glieder von regelkreisen. Z vgl Physiol 48:198–250

Wolf H, Büschges A (1995) Nonspiking local interneurons in insect leg motor control. ii. role of nonspiking local interneurons in the control of leg swing during walking. J Neurophysiol 73:1861–1875

Yakovenko S, Gritsenko V, Prochazka A (2004) Contribution of stretch reflexes to locomotor control: a modeling study. Biol Cybern 90(2):146–155

Yakovenko S, McCrea D, Stecina K, Prochazka A (2005) Control of locomotor cycle durations. J Neurophysiol 94:1057–1065

Zahedi K, von Twickel A, Pasemann F (2008) Yars: a physical 3d simulator for evolving controllers for real robots. In: Carpin S, et al (eds) Simulation, modeling and programming for autonomous robots (SIMPAR 2008), LNAI, vol 5325. Springer, pp 75–86